Universidade de Lisboa

Faculdade de Ciências

Departamento de Física

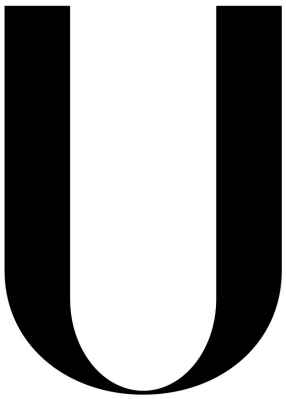

LISBOA

UNIVERSIDADE
DE LISBOA

The X-ray/Radio Correlation for Bulgeless Galaxies

João José Feio Calhau

Dissertação
Mestrado em Física
Astrofísica e Cosmologia

2013

Universidade de Lisboa

Faculdade de Ciências

Departamento de Física

The X-ray/Radio Correlation for Bulgeless Galaxies

João José Feio Calhau

Dissertação
Mestrado em Física
Astrofísica e Cosmologia

Orientadores: Professor Doutor José Manuel Afonso

2013

Abstract

The study of integrated light measurements in both the X-ray and Radio bands in galaxies allows for the identification of populations of new stars – and therefore, star formation processes – as well as markers for the presence of Active Galactic Nuclei.

Correlations between the X-ray and Radio emissions are observed for both galaxies with Active Galactic Nuclei (AGN) and in Star Forming galaxies. For the first case, the X-ray/Radio correlation seems to present different slopes for Radio-loud and Radio-quiet AGN and may be used to estimate the mass of the central black hole in these galaxies, while in the second case the correlation appears to support a link between the evolution of massive stars and their destruction, suggesting the possibility of using X-ray emission to determine the star formation rates.

This work presents a study on the presence of this correlation in bulgeless galaxies at intermediate redshifts ($0.4 \leq z \leq 1.0$). To this effect, the VLA and Chandra surveys for the COSMOS field are used and a recently selected sample of about 20000 bulgeless galaxies considered (Bizzochi et al. 2013). The bulgeless galaxies identifies in both the Radio (VLA) and X-rays (Chandra) surveys all have high enough luminosities for them to be defined as AGN and present a correlation that is identical to correlations determined for the general population of AGN by previous works.

Most of the bulgeless galaxy population (99%) is not detected by the surveys used. As such, stacking processes were used to extend the study of the X-ray/Radio correlation beyond the detection limits of these surveys. The correlation obtainned is similar to the ones found in previos works for galaxies dominated by star formation.

From these results, we conclude that most bulgeless galaxies do not possess AGN, as expected, and that the bulgeless galaxy population follows the same correlation as the general galaxy population.

Key Words: Bulgeless, Galaxy, Radio, X-ray, Correlation

Resumo

A análise das medições de luz integradas na banda dos Raios-X e do Rádio permite tanto a identificação de populações de novas estrelas – e, portanto, de processos de formação estelar – como a identificação da presença de núcleos galácticos activos (NGA).

Correlações entre as emissões nos Raios-X e no Rádio têm vindo a ser observadas tanto para casos de galáxias com formação estelar como para galáxias com núcleos activos. Para o primeiro caso, a correlação Raios-X/Rádio parece apresentar declives diferentes consoante o NGA tem forte emissão no rádio ou não e pode ser utilizada para estimar a massa do buraco negro central destas galáxias. No segundo caso, a correlação parece apontar para uma ligação entre a evolução das estrelas massivas (especificamente, estrelas binárias de grande massa com emissão nos raios-X) e a sua destruição (electrões acelerados por explosões de supernova), o que sugere a possibilidade de utilizar a emissão nos Raios-X para estimar taxas de formação estelar.

Este trabalho tenta averiguar e estudar a presença desta correlação em galáxias sem bojo a redshifts intermédios ($0.4 \leq z \leq 1.0$). Para o efeito, usou-se os levantamentos dos observatórios VLA e Chandra, bem como uma selecção recente de uma amostra de cerca de 20000 galáxias sem bojo (Bizzochi et al. 2013). As galáxias sem bojo detectadas em conjunto pelo Chandra e pelo VLA apresentam todas luminosidades que as classificam como NGA e a correlção delas obtida encontra-se em concordância com outras correlações obtidas em diferentes estudos para a população generalizada de NGA's.

A maior parte da população de galáxias sem bojo não é, contudo detectada directamente pelos levantamentos considerados. Este problema foi ultrapassado através do uso de métodos de stacking, o que permitiu a extensão da correlação para lá dos limites de detecção destes levantamentos. A correlação assim encontrada é idêntica à determinada noutros trabalhos para galáxias com formação estelar e sem NGA.

Destes resultados conclui-se que a maioria das galáxias sem bojo não possui NGA, como esperado, e que a população destes objectos obedece às correlações encontradas para a população geral de galáxias.

Palavras-Chave: Galáxia, Raios-X, Rádio, Bojo, Correlação

Preface

This dissertation is the result of the master's thesis project carried out at the Centro de Astronomia e Astrofísica da Universidade de Lisboa (CAAUL), in Lisbon, and is the last part of the Master's degree in Physics (specialization in Astrophysics and Cosmology) at Faculdade de Ciências da Universidade de Lisboa (Faculty of Sciences of the University of Lisbon – FCUL).

The CAAUL is a research center from the Faculty of Sciences of the University of Lisbon hosted by the Astronomical Observatory of Lisbon (OAL). Its research activity is concentrated in three main topics: “Origins and Evolution of Stars and Planets”, “Galaxies and Evolution of the Universe” and the “Optical Instrumentation for Astrophysics”.

The work done in this project falls under the group for “Galaxies and Evolution of the Universe” and consisted in the evaluation of the possible existence of a correlation between X-ray and Radio emission in bulgeless galaxies. The dissertation's work was done at CAAUL and benefited from the both the resources available there and the exchange of ideas and thoughts between several members of the research community.

I would like to thank the following persons: José Afonso for being my supervisor for both the dissertation and project itself and for the patience and interest demonstrated in the orientation process, helping with all the problems that appeared during the project and providing feedback on this dissertation. Also thanks to João Retrê and Manuel Menezes for providing valuable instruction on how to understand and run the necessary software. Finally, I would like to also thank Marco Grossi for the explanations regarding the stacking process and Luca Bizzocchi for providing and explaining the bulgeless galaxy selection catalog instrumental in this work.

Table of Contents

List of Tables

List of Figures

1. Introduction

Galaxies have always had a “visible” role in Human History. Initially, of course, such presence was made in the form of our own Milky Way galaxy, particularly the arm which is visible from the Earth's surface when one peers up to the sky at night. Its influence is so deep it makes its way into popular culture. In Portugal and Spain, the Milky Way is known has Santiago's Road, the way souls follow on their journey to heaven. Some tribes of Africa, on the other hand, saw the arm of our Galaxy as the support structure upon which the entirety of the night sky rests – without it, all of the heavens would fall on our heads.

Our knowledge of the Universe and galaxies in particular would eventually evolve. For a long time it was thought that galaxies were objects within our Milky Way and, for a time, even shared the designation of “nebula” with the clouds of gas and dust that are associated today with such name. In reality, galaxies are objects far beyond the Milky Way and not at all clouds of gas and dust. Although these components are present in varying quantities – particularly gas for younger galaxies and dust for the older ones (it's important to remark here that this applies in a proportional context; that is to say, an older galaxy has more dust in proportion to gas than a younger one. An old galaxy, such as an elliptical galaxy, has very little gas and dust on the whole)-, a galaxy is more than that: a physical system of millions of stars held together by the power of gravity.

The Universe is populated by a great variety of different galaxies, differing in mass, shape, size and so on. With such diversity, there are patterns that start to emerge and, naturally, we try and group these objects according to these recurring characteristics. One way of doing so is through the Hubble classification method. This way of classifying galaxies was developed by Edwin Hubble in 1926 and further developed in 1959 by Gérard de Vaucouleurs. It's a morphological classification and separates the galaxies in three major classes based on their visual appearance (see figure 1). Galaxies are, therefore, separated into elliptical galaxies, spiral galaxies and lenticular galaxies.

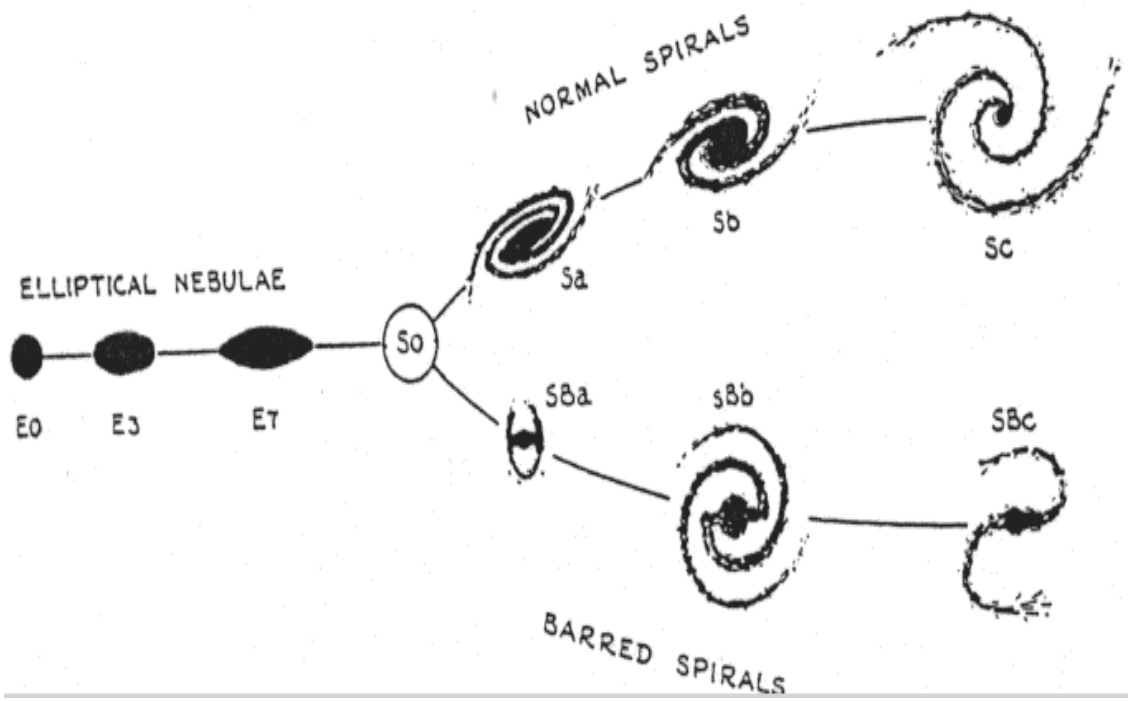

Fig. 1: The original Hubble classification diagram (from Hubble, 1958). Note that here, elliptical galaxies are still referenced as “nebulae”. It would only be later that galaxies would be recognized as independent objects, beyond the Milky Way.

The characteristic shape of the Hubble diagram earns it the name of “tuning-fork diagram”. In it, elliptical galaxies are denoted by the letter E and are defined by being having featureless light distributions and appearing as ellipses in images. The higher the number following the letter E, the more elliptical the galaxy is.

Spiral galaxies, on the other hand, are attributed the letter S and feature a flat disk with stars arranged in the shape of a spiral of two or more arms and a central bulge reminiscent of elliptical galaxies. Unlike elliptical galaxies, spiral galaxies are not classified with a number but rather with a letter, from “a” to “c”. A spiral galaxy Sa is characterized by having tightly-wound arms and a large central bulge, whereas a Sc spiral galaxy has loose spiral arms and a fainter, less defined central bulge. If a galaxy shows the presence of a bar-like structure across its bulge, it is named as a barred spiral and receives the classification of SB, with the lower case letter defined in the same way as to normal spiral galaxies. For galaxies that stand between two different subclasses, it's common practice to assign a second lower case letter to specify how the galaxy stands in the overall classification. An Sbc galaxy would, therefore, be a galaxy between Sb and Sc. Our Milky Way itself is thought to stand as a SBb, a barred spiral with well

defined arms.

Finally we come to the third and final class of galaxies: the lenticular galaxies. These are galaxies with a central bulge but whose disk is not arranged in spiral arms, instead being smooth and featureless. Their designation is S0 and they stand at the center of the diagram. Their bulge is the primary source of light and their overall appearance makes them very difficult to distinguish from elliptical galaxies when viewed face on.

There are, of course, galaxies that do not fit Hubble's classification criteria. These objects are dubbed irregular galaxies and are divided into two subclasses: Irr I and Irr II. The first are galaxies with no obvious shape or symmetry but which present defined clusters and stars in their structure. On the other hand, Irr II galaxies also have no defined symmetry but do not have clearly resolvable clusters or stars. An example of these types of galaxies are the Magellanic Clouds, although, because the Large Magellanic Cloud seems to have some spiral like characteristics, it is sometimes classified as Sm (from Magellan Spiral), with the Small Magellanic Cloud being given the symbol Im (for Magellan Irregular). They are usually placed at the end of the spiral fork of the diagram.

The Hubble diagram is in all probability the most used system for classifying galaxies, both for amateur and professional astronomers, but for all its convenience it is not without flaws. The main problem is that the classification of the galaxies is a subjective process and it is sometimes difficult to agree on which subclass a given galaxy is to fall into. Furthermore, because its based solely on optical morphological qualities, many characteristics of the galaxies are ignored when applying this classification method: while it does help in organizing the galaxy class in general, it does little to inform us on what exactly happens within those galaxies, what processes take place and why, and what evolutionary path these objects have followed since their creation. To do that, other methods are necessary.

1.1 - The Formation of Galaxies

The Cosmic Microwave Background gives us some clues as to what the Universe might have been like just after the recombination era. From it, it's been deduced that the Universe of that time (z~1000, approximately 370000 years after the Big-Bang) consisted of matter almost uniformly distributed through space. The minute fluctuations in density that prevented the gas distribution from being completely even are important, for they lead to the gravitational collapse that would form the galaxies. The accepted models of the Universe maintain that dark matter dominates everywhere but in the inner parts of the larger galaxies. It stands to reason then, that the gravitational forces responsible for gathering matter into galaxies are due to the dark matter - and that ordinary matter merely “goes with the flow”.

The formation of visible galaxies is expected to follow the formation of dense concentrations of dark matter. When dark matter forms these dark halos, galaxies then form in these halos as a consequence of gas infall – followed by star formation due to gravitational collapse (Fall and Efstathion, 1980; White and Frenk, 1991). As the early Universe evolved, small condensed structures would develop first and subsequently merge into progressively larger ones, in a hierarchical process. The present day galaxies can, then, be simply the smallest structures to have survived isolated from such times (Peebles, 1974; Peebles, 1980).

Information about the way the early Universe was structured is possible to obtain from the distribution of matter on scales larger than that of clusters of galaxies, because on these scales the gravitational clustering has not yet been able to erase the initial conditions, so the structures at this scale still conform to the linear regime (that is to say, the density fluctuations are merely an amplified form of the original perturbations).

Numerical simulations have tried to study the development of structures in the presently accepted Cold Dark Matter (CDM) universe theories on scales comparable to those of groups of galaxies (Frenk et al, 1988, Carlberg, 1988). While they can't give any detailed information on individual galaxies, these simulations all show that in the denser regions of the Universe, small dark halos form first and then merge rapidly into larger ones, resulting in the appearance of large halos. In low density regions the mergers are less important and, instead, accretion of diffuse matter is what plays into the growth of

these dark matter structures. Therefore, in dense regions it is mergers that are responsible for the formation of galaxies, whereas in low-density regions this process is surpassed by accretion processes in terms of importance. In both cases, the dark halos formed in the simulations appear to be isothermal which is encouraging, since the disks that form from them would have nearly flat rotation curves, something that is in agreement with observational data (these simulations also reproduce the Tully-Fisher and Faber-Jackson relations between mass and virial velocity of galaxies - Frenk et al. 1988).

Later simulations (Katz and Gunn, 1991; Katz, 1992) showed that the process encompasses an initial chaotic stage during which mergers build up a dark halo and a stellar spheroid followed by a more prolonged period during which the remainder of the gas forms a disk. The formation of the disk is a chaotic process and the initial conditions greatly affect the final disk-to-spheroid relation. Small satellite systems may form during the early stages of the halo formation and survive, continuing interacting with the disk.

1.1.1 - Disk Formation

Disks are common structures in the Universe and are formed through the conservation of angular momentum in a system collapsing under gravity, leading to arrest of the collapse by rotational support. Galactic disks are no exception to this rule.

In 1962, Eggen et al. proposed that galaxies, in particular disk galaxies, form through the collapse of a large gas cloud. The collapsing process forces the gas to form a rapidly rotating disk. The discoveries made since then have invalidated this hypothesis, since, as it's already been said, galaxies seem to form from smaller structures to larger ones. The angular momentum of the matter which will eventually form the disk of a galaxy originates in a similar way to that of dark matter halos: from tidal forces surrounding large scale structures (Hoyle, 1949) and its magnitude is considered to be a scaled down version of that of dark matter (van der Bosch, et al. 2002). While its distribution is less well understood, there are some simulations that try to shed a light on the subject (Sharma and Steinmetz, 2005).

Early simulations assumed that there was a conservation of the angular momentum during the collapse and typically found that disk galaxies lost a good part of their angular momentum and, as a result, were smaller than expected (Navarro et al. 1994, 1995). However, newer calculations show the expected angular momentum (most likely due to the inclusion of feedback processes in the simulations) and lead to disks of comparable sizes to those observed in present day galaxies (Steinmetz and Navarro, 2002; Thacker and Couchman, 2001).

Stellar disks are not razor thin. The origins of the vertical extent of galactic disks remains a topic of research, but there are already some theories about the process:

- Disk Accretion: Because galaxy formation is hierarchical, it can be expected for the disk to accrete preexisting smaller stellar systems in its life. The stars of these smaller systems are found in some simulations to form a thickened disk structure in the same place as the original galactic disk. The friction and tidal forces these stars experience force them to fall into orbit on the plane of the galactic disk (Abadi et al. 2003).
- Early Chaotic Accretion: In different simulations it has been fund that many thick disks form from accreted gaseous systems during a chaotic period of merging in the early life of the new galaxy (Brock et al. 2004).
- Dark Matter Substructure: Several studies have shown that disks can survive in the chaotic environment of dark matter halos hierarchical formation. Interactions with orbiting dark matter substructures seem to greatly contribute to the thickening of the galactic disk (Font et al. 2001; Kazantzidis et al. 2008).
- Molecular Clouds: Massive molecular clouds can gravitationally scatter clouds that happen to pass by them, transferring some of their orbital energy in the plane of the disk into motions perpendicular to that of such plane, resulting in the thickening of the disk (Spitzer and Schwarzchild, 1953).

Most likely, rather than existing merely one correct way for the formation and thickening of the disk, it's probable for the true process to be a combination of all of these hypothesis.

1.1.2 - Mergers and the formation of Bulges

Bulge-like structures can form either in result of cataclysmic events that destroy preexisting stellar systems, like violent mergers, or through the evolution of galactic disks. The first process is a natural consequence of hierarchical galaxy formation (smaller systems merging to form larger ones), while the second is due to the dynamics of the galactic disk itself.

There has been a lot of attention dedicated to the influence of mergers in the evolution of galaxies. Evidence of such mergers exist even in our own Milky Way – the satellite dwarf galaxy of Sagittarius is orbiting our galaxy at an almost right angle to the disk and is currently passing through it, its stars being torn off and joining our galaxy's halo. This provides the host galaxy with new stars, along with a fresh supply of gas and dark matter – with the merging processes usually being detected through warps in the morphology or streams of matter coming out of the galaxies.

It's common practice to divide galactic bulges in two different classes: classical bulges and pseudo-bulges (Kormendy and Kennicutt, 2004). Classical bulges have properties similar to those of elliptical galaxies and earn their name due to the their morphological similarity to the view historically held for these structures. These bulges are composed mainly by old population II stars (metal-poor stars), which give them their characteristic red color. These stars have random orbits compared to the plane of the galaxy, giving it its distinct spherical form. Classical bulges are thought to be formed by the collision of smaller structures (Benson, A. J., 2010), which disrupts the path of the stars, throwing them into random orbits. During the merger, gas clouds are likely to go into collapse, triggering the formation of new stars, due to the shocks from the merging process. Fully formed bulges tend to have almost no star formation, since they are extremely poor in gas and dust.

Pseudo-bulges, or disk-bulges, on the other hand, are structures whose stars do not have such random orbits. Rather, they orbit in almost the same plane as the outer disk, making pseudo-bulges more similar to spiral galaxies than elliptical ones. To make things even more interesting, disk-like bulges differ even further from classical ones by having higher star formation rates and often presenting a spiral structure much like the galactic disk, which may imply that these structures share similar formation processes or that

pseudo-bulges are formed from the secular evolution of the disks themselves (Benson, A. J., 2010).

1.1.3 - Elliptical Galaxies

Elliptical galaxies can reach to be the most massive objects in the Universe. They are, just like classical bulges in spiral galaxies, composed of stars with random orbits and having very little dust. Elliptical galaxies are often found in crowded regions of the Universe, often at the center of clusters of galaxies, being the most massive object there, much like the Sun in our own Solar System.

It's thought that the main process through which these galaxies form are mergers between smaller galaxies of comparable mass. These are the Major Mergers. When such a process takes place, the two galaxies collide violently, often at speeds of about 500 kilometers per second.

The effects of the merger depend on a collection of different parameters, from collision angles to the composition of the intervening galaxies and are currently the focus of active study, given the importance of these events in the understanding of galactic evolution. During the merger, gas, stars and dark matter of each galaxy become influenced by the approaching neighbor. This results in the deforming of the galaxies (NGC 4038/4039 being probably one of the most illustrative examples of this consequence – figure 2), with the accompanying change in the gravitational potential – which happens so quickly that star orbits are thrown into disarray, in a process known as violent relaxation.

Fig. 2: NGC 4038 and NGC 4039, also known as the Antennae galaxies are one of the most illustrative examples of galaxy mergers. Credit: NASA, ESA, and the Hubble Heritage Team STScI/AURA)-ESA/Hubble Collaboration. Acknowledgement: B. Whitmore (Space Telescope Science Institute) and James Long (ESA/Hubble).

This can turn the well-defined motions of the stars in the disk into random orbits, leading to the formation of a spheroid. This process is still poorly understood and several studies are underway to try and understand it better (e.g. Arad and Lyndell-Bell, 2005). Furthermore, major mergers don't always originate elliptical galaxies and the production of these final objects seem to be dependent on multiple variables: major mergers of purely stellar disks do not look like elliptical galaxies even if they are considered spheroids – which may imply that the merger needs a minimum amount of gas present for the final result to be an elliptical galaxy. Also, although mergers with a mass ratio of $\mu \equiv M_2/M_1 \geqslant 0.25$ destroy the disks and leave a spheroid remnant in their place, lower mass ratios tend to leave the disks intact, although thickened, and a merger of systems very rich in gas (and with mass ratio greater than about 0.5) may allow for the reformation of a disk after the collision (Robertson et al. 2006).

Major mergers are the stage of some of the most intense star formation rates known to Man. Although, during the collision, stars almost never come into direct contact with each other, the same cannot be said for gas clouds. The shock waves born from these collisions excite the gas in the nebulae and are the “spark” needed for a new burst of star formation to take place. Because of this, most of the gas available for the new galaxy is consumed in the process, giving way to the elliptical galaxies we see today, poor in gas and with almost no new stars.

1.2 – Key Processes Shaping Galaxy Evolution

As is apparent from the sections above, different types of galaxies (and different types of components, really), encompass different kinds of evolutionary processes. Whereas classical bulges and elliptical galaxies are formed by more violent, catastrophic events, stellar disks and pseudo-bulges change more slowly, due to the natural evolution of the galactic system (secular evolution). However, this doesn't mean that there is a clear distinction on which processes affect a galaxy's evolution the greatest. In fact, the evolution of a galaxy is the result of the combination of both mergers and secular evolution; the only difference between elliptical galaxies and spiral galaxies is the magnitude by which these processes have influenced the shaping of the galaxy itself.

However, the direct study of these processes is pretty much impossible, given the timescales involved in them. As is often the case with astrophysical processes, researchers are forced to look for related processes that might give us clues to the evolution of a galaxy rather than trying to observe a merging directly, for example. Two of these indirect processes are Star Formation and Active Galactic Nuclei. Both are tied to secular and merging processes: Star formation may occur due to the natural evolution of the stars and gas in the disk (Supernovae explosions, gas compression due to shock waves) or due to the massive instabilities generated by the collision between two galaxies (which literally throws gas nebulae into each other and provokes gravitational collapses) and the massive black hole of an AGN is formed and enlarged by both merging processes joining lower mass black holes together and by secular

evolution of the galaxy which condenses material in the central bulge and provides the "fuel" that lights the AGN in an active galaxy.

It is the purpose of this section to briefly describe both Star Formation processes and Active Galactic Nuclei.

1.2.1 - Star Formation

Typically, stars form in interstellar gas clouds. These clouds are sometimes called molecular clouds due to the high amount of molecular hydrogen present in them – around 70% - with the remainder of the gas being mostly helium and trace amounts of heavier elements.

An interstellar cloud of gas remains in hydrostatic equilibrium as long as the pressure from kinetic energy of the gas is enough to counter-balance the potential energy of the cloud's gravitational force. This is well illustrated by the Virial Theorem, which states that a system will remain in thermodynamic equilibrium if the gravitational potential energy is equal to twice the internal thermal energy (and, therefore, the kinetic energy):

$$2\mathrm{K} = -U$$

Where K is the kinetic energy and U is the gravitational potential energy.

If the cloud has enough mass, the gas pressure is not enough to keep the matter from falling into itself and the cloud undergoes gravitational collapse. The limit above which the mass triggers this event is called Jean's mass and depends on the temperature and density of the gas cloud,

$$M_J = \frac{5\mathrm{k}_B T}{m_H G} R_J$$

Where k_B is the Boltzmann constant, T is the temperature, m_H is the mass of a hydrogen atom, G is the gravitational constant, R_J is the Jeans radius and M_J is the Jeans mass. This

mass is, typically, of orders of magnitude from thousands to tens of thousands of solar masses and coincides with the typical mass of an open cluster of stars.

The shock waves from the merging process induce variations in the cloud's gas density and radius and force the system to surpass the limit imposed by Jean's mass, triggering the gravitational collapse. This is what is called triggered star formation and can be observed even in the absence of collisions between clouds when a nearby supernova sends shocked matter into the cloud at extremely high speeds.

The protostellar cloud collapses until the cloud compresses enough to become opaque to its own radiation. At this point the energy must be removed through some other means and that is accomplished through radiation in the infrared band, due to the heated dust particles within the cloud, to which the cloud itself is transparent. The frontier inside the cloud where the collapse is halted is called the First Hydrostatic Core and continues to increase in temperature, forming a protostar. The gas falling into this opaque region collides with the core and creates shock waves that further heat the core. After the temperature of 2000 K is reached, the thermal energy is sufficiently high to dissociate molecular hydrogen. What follows is the ionization of the hydrogen and helium atoms. When the density of the in-falling gas falls bellow 10^{-8} g/cm^3, the remaining cloud is sufficiently transparent to allow the energy radiated by the protostar to escape. This, combined with the convection processes of the protostar itself, allows it to contract even further, a process which continues until the gas becomes hot enough for the internal pressure to support the protostar against gravitational collapse. The protostar has reached hydrostatic equilibrium.

The remainder of the material left-over from the process coalesces into an accretion disk and continues to fall into the protostar. When the density and temperature reach the required levels, the protostar begins the fusion of deuterium and the pressure from the resultant radiation slows the collapse. This accretion process stops when the surrounding gas and dust disperses – at this point the star becomes a pre-main sequence star (PMS). The energy of the PMS is the gravitational collapse. The contraction proceeds until the Hydrogen fusion starts in the core of the newly formed star. Here, the radiation coming from the star clears the remaining gas and dust from its vicinity and the star enters the mains sequence.

The study of star formation, particularly its rates and history through the host galaxy's

life is important, since it allows for the understanding of what the galaxy went through since it's formation (a rampant process of star formation may the sign of a recent merger, as has already been said). The problem with studying star formation is that many of the elements of this process are impossible to observe in the optical band of the electromagnetic spectrum. The protostellar stage of star formation is almost always obscured by the dense cloud of gas and dust that is the left over from the original molecular cloud. However, as stated before, the cloud is transparent to infrared radiation so, in theory, it should be possible to observe star forming regions in the infrared band. Unfortunately, our planet's atmosphere complicates matters considerably by being almost entirely opaque from 20μm to 850μm (see figure 3).

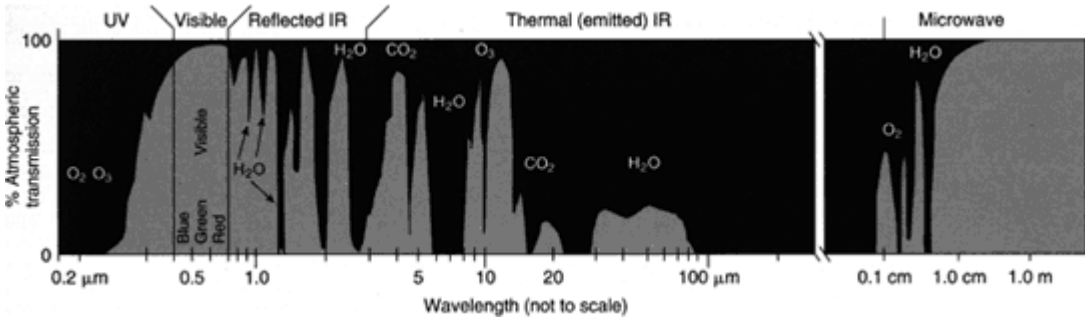

Fig. 3: The “Atmospheric Windows”, detailing the regions of the electromagnetic spectrum to which Earth's atmosphere is opaque. Note that a big fraction of the region for thermal infrared emissions is blocked by our atmosphere. Original image by NASA.

Furthermore, the use of the infrared band as a tracer for star formation rates (SFR) depends on the contributions of the young star's ultraviolet emissions to the heating of the dust in the molecular cloud, as well as the optical depth of the dust itself. This contribution is often difficult to estimate (Buat and Xu, 1996; Vattakunnel et al. 2011).

Another way to detect SFR is through the nebular emission lines, which re-emit the integrated stellar luminosity of the young stars. This is usually done through the Hα line but this method is sensitive to extinction and is vulnerable to contamination by non-thermal optical emission, something that is difficult to separate from the emission due solely to star formation.

The UV, optical and IR observation windows are still the most used bands for studying star formation in galaxies but there are other options available for the study of stellar

and galactic evolution: the Radio and X-ray emission.

When it comes to star formation, the emission at radio frequencies is due mainly to two different processes: synchrotron radiation from supernova explosions and thermal bremsstrahlung from HII regions. We will explore this processes in section 1.4.

The relation between radio luminosity and SFR has been the focus of several different studies (e.g. Yun et al. 2001; Schmitt et al. 2006). The observables are sensitive to the number of the most massive stars and provide a direct measure of the instantaneous SF above a certain mass. There is also a very tight correlation observed between IR emission and radio emission at low and high redshifts (Bell, 2003; Mao et al. 2011). However, there is no clear theoretical relation between radio luminosity and SFR and the relations used are derived empirically.

As for the X-ray emissions, the link with star formation (SF) is established through High Mass X-Ray Binaries (HMXB), young supernova remnants and hot plasma associated with SF regions. The HMXB have evolutionary time scales that do not surpass years 10^7 because, since they are very massive, they consume the available Hydrogen much faster and are much shorter-lived, having a lifetime comparable to the duration of the star formation process. Although some problems arise in the soft-band regarding the separation between the contribution to the emission by star formation and the contribution of gravitationally heated gas, X-ray emission are considered a good estimator of SFR in galaxies where a supermassive black hole is not active (galaxies without Active Galactic Nuclei).

1.2.3 - Black Holes and Active Galactic Nuclei

Merging processes may be responsible for another characteristic of some galaxies: the activity of a central supermassive black hole (SMBH).

Active Galactic Nuclei, or AGN, are compact regions at the center of galaxies with a much higher luminosity than normal. It is believed that these phenomena are a consequence of a supermassive black hole going through a phase of intense matter

accretion. It is generally accepted that AGN are composed of at least three distinct parts, present in figure 4:

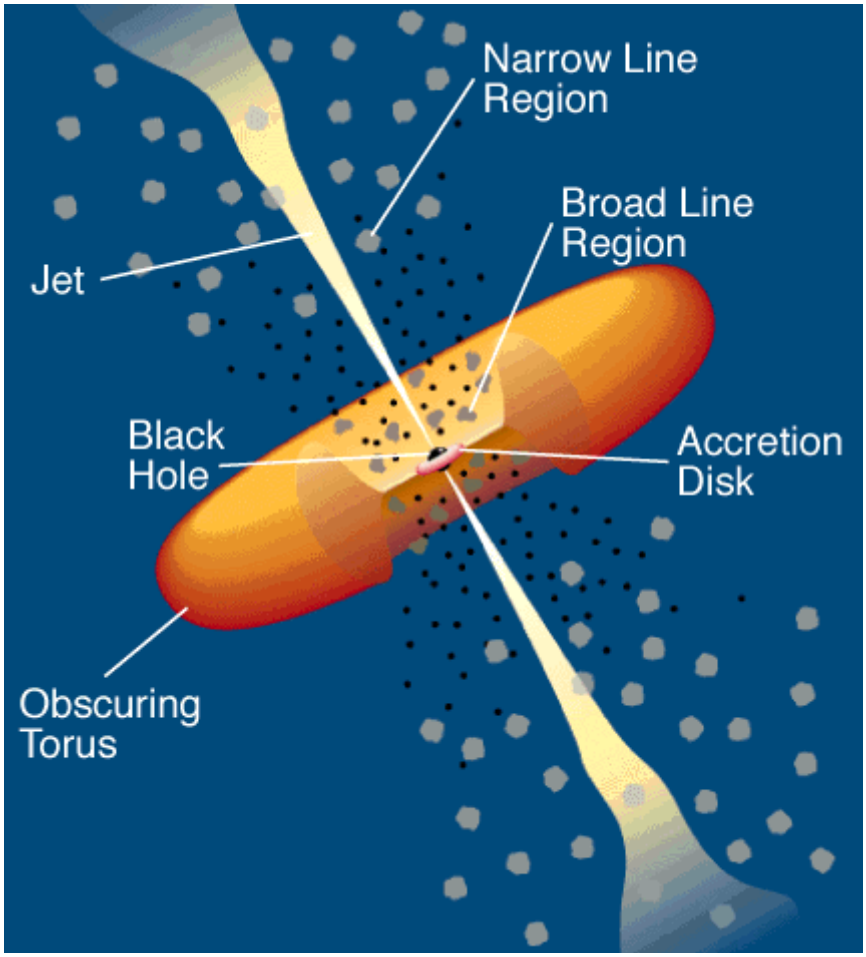

Fig. 4: Schematic of an AGN by C.M. Urry and P. Padovani.

- Central Supermassive Black Hole
- Accretion Disk – Formed by the material falling into the black hole, the dissipative processes in the accretion disk transport matter inwards and angular momentum outwards, which causes the disk to heat up. A corona of hot material forms above the disk and provokes the inverse-Compton scattering of photons, which are radiated in the form of X-rays.
- Relativistic Jets – relativistic jets emerge from the AGN at the center of active galaxies. The material from the accretion disk is captured by the twisting magnetic fields and collimated into a jet-like shape., although the exact way these artifacts are produced is not completely understood. Relativistic jets can,

however, be studied through their radiation, most importantly, for us, on the radio band, through the emissions due to the inverse-Compton scattering process and synchrotron radiation.

For some time, it was thought that AGN were responsible for all but a part of a larger family of active galaxies, the others being Seyfert galaxies, Blazzars and Quasars. Today it is thought that rather than being different types of objects, the fundamental thing that changes from AGN's to Quasars is the orientation, or the angle they make with our line of sight (as illustrated in figure 5).

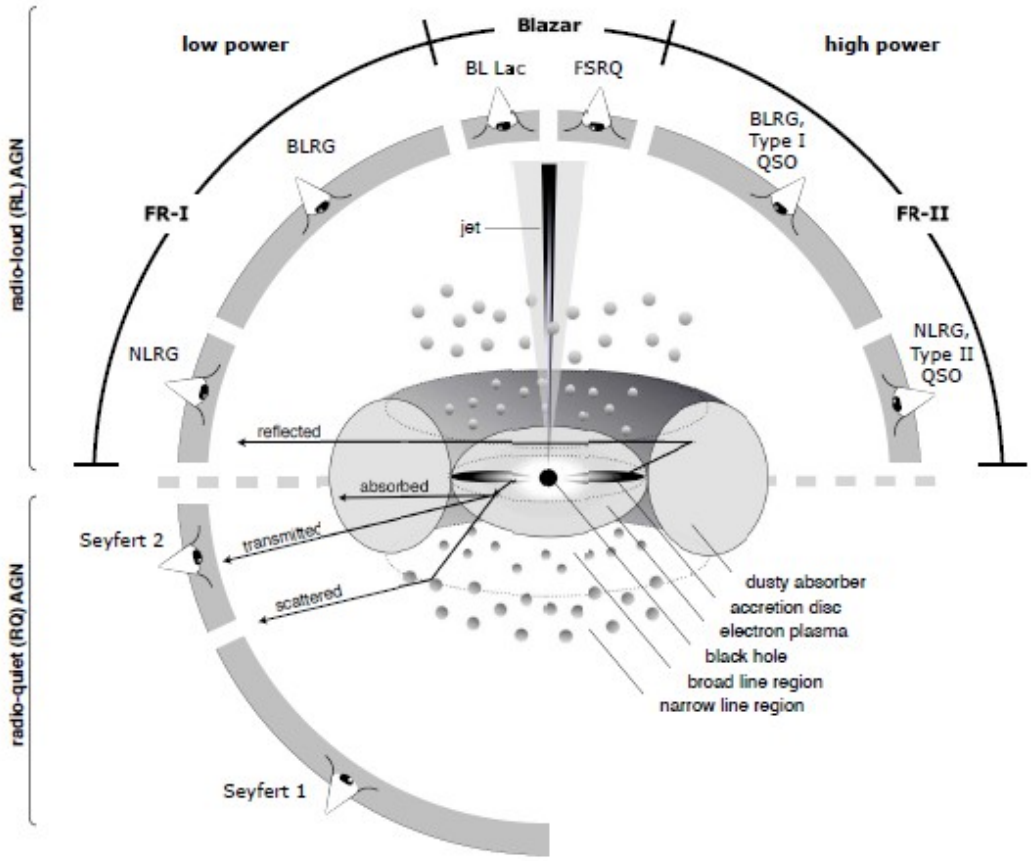

Fig. 5: Schematic illustrating how line of sight affects our perception of an AGN. Source: Beckmann, V. et al. 2013.

Observations so far seem to suggest that most galaxies have black holes in their center, with quasars reaching black hole masses of 10^9 solar masses observed at redshifts higher than z=6 (Fan et al. 2006). The merging hypothesis holds that supermassive black

holes may have been formed by the accretion and fusion of stellar remains (Haiman, 2004) or through collisions of young, dense stellar clusters (Omukai et al. 2008). However, there are some problems with these ideas: for the first one, numerical simulations imply that gas densities in the vicinity of black hole from stellar remnants is low, which makes the hypothesis of accretion difficult, while the second scenario can only happen if the Universe is enriched with heavier elements from the first stars and the simulations return black holes of 10^3 solar masses instead of the observed ones at high redshifts.

A relatively recent alternative may be the hypothesis that primordial black holes form through the direct collapse of proto-galactic haloes so long as the fragmentation of these haloes is avoided (Bromm and Loeb, 2003; Schleicher et al. 2010) and most of the material is allowed to accrete onto the center.

The exact process by which these objects are formed is still unclear but their study is an important part of learning how galaxies form and evolve. The existence of strong correlations between the masses of these black holes and the properties of their host galaxies – velocity dispersion (Ferrarese and Merritt, 2000), amount of globular clusters (Buckert and Tremaine, 2010) or dark matter halo (Ferrarese, 2002) – suggests a relation between the forming galaxies and supermassive black holes.

Feedback from AGN, for example, has the potential to directly link the properties of SMBH and host galaxies, which would provide a relation between the SMBH and galaxy mass or velocity dispersion. How this feedback works is not yet completely understood, but it is likely that AGN are responsible for heating the cooling gas through radiation, reducing the rate at which the latter is able to cool, while, at the same time, originating winds driven by radiation that may impact on the development of the galaxy itself (Benson et al. 2003). The radiative feedback alone is able to regulate the cooling of the gas so that models agree with observations, but fails when it comes to restricting the growth of black holes. If we consider no other means of feedback, these black holes end up being too massive for a given galaxy when compared with observations. However, if one includes mechanical feedback from the radiation winds, this problem is eliminated (Ciotti et al. 2009; Springel et al. 2005). Numerical simulations by these authors seem to show that AGN can expel gas from a galaxy and establish connections between the central black hole and galaxy properties. Nevertheless, some problems persist, as the

mechanical feedback can deplete the gas of a galaxy to a greater degree than expected if the process has high efficiency, while leaving gas available for late star formation in case of low efficiency, producing elliptical galaxies with blue cores, which does not agree with reality.

1.3 – The Case of Bulgeless Galaxies

Hubble's morphological classification scheme has become so ingrained in the idea usually associated with galaxy, that people traditionally associate two elements with the object itself: a central, concentrated spheroid structure – the bulge – and a disc-like stellar distribution, often associated with spiral arms. A galaxy can be classified according to the relative contribution of these two components to the total light emitted by the system, while finer classifications include contributions from other elements (bars, spiral arms).

One could consider different types of galaxies as differing only on the importance of each of these components. So an elliptical galaxy would be a galaxy dominated by the bulge component, while spiral galaxies would have a more prominent disk presence. This view is exacerbated by the fact that bulges are now seen as a heterogeneous group with pure, spheroid systems – classical systems, dynamically and photometrically similar (the light we receive from one object has the same properties as the one received from a different one) to elliptical galaxies but with different kinematic properties (Davies and Illingworth, 1983) – and “pseudo” bulges, characterized by disc-like properties (Kormendy and Kennicutt, 2004).

But if we consider elliptical galaxies as a system where the classical bulge component is the overwhelming force behind the morphology of the galaxy, then surely there could be the opposite case: a system where the disk is the dominant feature morphologically and with a pseudo bulge that shares common characteristics with that prominent disk.

These are the bulgeless galaxies (figure 9) and they are peculiar objects in the sense that they do not quite fit the current models for galaxy formation and evolution.

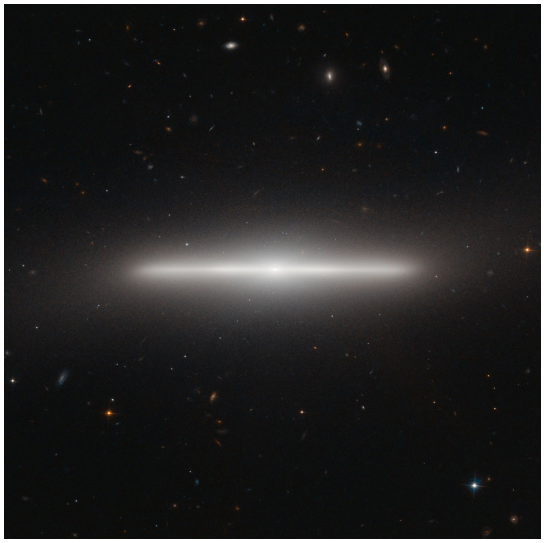

Fig. 6: A bulgeless galaxy (NGC 4452). Credit: ESA/Hubble & NASA.

Earlier in this work we have touched briefly on the accepted mechanisms that lead to the formation of a galactic system: early star formation takes place in disks, which form due to the conservation of angular momentum. Bulges form from the physical processes that remove angular momentum from stars and gas, with classical bulges being associated with violent processes like major mergers, and pseudo bulges being related to secular evolution in the disk component (the original disk is unstable and reaches equilibrium with the rearranging of part of the gas and stars, that concentrate in a central, denser structure).

Considering these points, a bulgeless galaxy must then be a system where the evolution is characterized by a lack of major mergers, with the galaxy absorbing only much smaller satellites (a ratio of 1:10 from Hopkins et al. 2011, although other values have been suggested). Since they cannot have been formed by major merging processes, which would form a classical bulge, the history of bulgeless galaxies must be dominated by purely secular – slow, internal – processes and one would expect them to be a minority, given the way the hierarchical formation theory defends galaxies are born. However, there is a large presence of these disk galaxies in the overall galaxy population, which poses a problem, since they can't have been formed through the usual methods.

The problem becomes even worse if one tries to include bulgeless galaxies in the

simulations for the formation of galaxies based on the cold dark matter model currently accepted: the galaxies obtained are too small, too dense and have a lower angular momentum than expected (Steinmetz and Navarro, 1999; Mayer et al. 2008). If the angular momentum was to be conserved during the fall of the gas towards the center of the galaxy, it would in principle be sufficient to form large galactic disks. However, the cooling of the progenitor halos of dark matter at high redshifts lead to the condensation of the gas in their inner regions and the dynamical friction between orbiting satellites dissipates the angular momentum (Mo et al. 1998; D'Onghia et al. 2006). Furthermore, the loss of angular momentum can also be due to secular processes from the evolution of disks and bar instability. The fact that these are more easily triggered in disks made compact by the partial loss of angular momentum only adds more fuel to the proverbial fire.

In an effort to investigate this issue, Fontanot et al. (2011) were able to simulate the formation of galaxies and obtain results in which galaxies without classical bulges made up to 14% of the total mass of galaxies in the range $10^{11} < M_*/M_{solar} < 10^{12}$. However, this result was obtained by considering a perfect angular momentum conservation (no dissipative processes at all) and by dismissing the effects of the detailed structure of disks.

The solution, so far, seems to fall along the lines of including fine tuned feedback effects in the small high-redshift dark matter halos, in order to avoid early gas cooling (Governato et al. 2010) and prevent the cascading of events that lead to the so called “angular momentum catastrophe”. But the study made by Fontanot et al. (2011) is particularly interesting because the model bulges gain mass as a result of both mergers and secular processes. Considering that classical bulges are considered to be inherently related to mergers and “pseudo” bulges associated with disk instabilities, there might exist the possibility of bulges being, themselves, composite systems, with a pseudo-bulge hiding a classical component and vice-versa.

If there is one thing that is certain is that the formation and evolution of bulgeless galaxies is not yet well understood, and researchers can't even seem to agree on whether or not the feedback processes are the right way of bypassing the angular momentum problems – although this method is the most widely accepted.

In order to further our understanding of these mysterious objects it is necessary to have

a large sample of bulgeless galaxies, with great observational coverage, with which to try and characterize the overall population and compare them to the general galaxy population (identifying where they depart from known galaxy regularities and trying to understand the process that lead to their origin in the currently accepted hierarchical Universe model).

1.4 – Light from Galaxies

It is important to understand the mechanisms for the emission of radiation, specially in the bands used in this work. This is because for astronomers and astrophysicists, the only way to obtain any information on the object being studied is through the analysis of the light (radiation) that reaches us. Knowing the processes which lead to the emission of such light enables researchers to stipulate on what is happening with the object being studied and how it may have arrived at its current state.

In galaxies, most of the light that reaches us is stellar in origin, the total light being the integrated spectrum of the stars. But, although a galaxy has quite a number of stars – 10^9 to 10^{11} of them -, the bulk of the emission is received in the optical band of the electromagnetic spectrum. As has been mentioned in the previous sections, the optical band is not the best for studying, since most of these processes take place in dust-rich environments, which force researchers to rely on the Infrared, X-ray and Radio bands. Although the last two receive only minor contributions from stars themselves when it comes to the total emission in a galaxy, there are mechanisms which contribute to the total galactic emission in X-ray and Radio wavelengths (Supernovae and HMXB systems, when it comes to processes related to stars, and processes related to AGN, as detailed in the previous sections).

Given this fact, this section is dedicated to the processes through which galaxies may emit radiation in the x-ray and radio bands.

1.4.1 - Compton Scattering

Compton scattering is an example of inelastic scattering, being usually applied to the electrons of an atom – although it may also happen with atom's nuclei. It was first observed by Arthur Compton in 1923 and earned him the Nobel Prize for Physics in 1927.

The interaction between photons and electrons at high energies (~500keV) result in the transfer of energy from the photon to the electron, which forces the photon to change the direction of its movement in order to conserve the total momentum of the system.

Derivation of the expression for the Compton scattering is a relatively simple process:

Let us consider, like Compton did originally, that the interaction between these two kinds of particles is made solely on a one photon-one electron basis. The conservation of energy states that the total energy of the system before and after the scattering must be the same so,

$$E_\gamma + E_e = E_{\gamma'} + E_{e'}$$

where E_γ is the energy of the photon before the scattering, E_e is the energy of the electron before the scattering and $E_{\gamma'}$ and $E_{e'}$ are the energies of the photon and electron after the scattering, respectively.

If we assume the electron to be at rest prior to the scattering event, then the conservation of momentum requires that the particles be related by

$$\vec{p}_\gamma = \vec{p}_{\gamma'} - \vec{p}_{e'}$$

On the other hand, the energies can be expressed in terms of frequencies with

$$E_\gamma = hf$$

where h is Planck's constant.

Since we are treating the electron before the scattering as being at rest, its total energy is given merely by its rest mass so,

$$E_e = m_e c^2$$

However, this changes after the process and the total energy of the electron is now represented by the relativistic energy-momentum relation:

$$E_{e'} = \sqrt{(p_{e'} c)^2 + (m_e c^2)^2}$$

Making the necessary substitutions into the expression for the conservation of energy we obtain

$$hf + m_e c^2 = hf' + \sqrt{(p_{e'} c)^2 + (m_e c^2)^2} \Leftrightarrow$$

$$\Leftrightarrow p_{e'}{}^2 c^2 = (hf - hf' + m_e c^2)^2 - m_e{}^2 c^4 \quad (1)$$

With this we now know the magnitude of the momentum of the scattered electron. From here it's just a question of using the conservation of momentum to obtain

$$p_{e'} = p_\gamma - p_{\gamma'}$$

By the scalar product we have,

$$p_{e'}{}^2 = \vec{p}_{e'} \cdot \vec{p}_{e'} = (\vec{p}_\gamma - \vec{p}_{\gamma'}) \cdot (\vec{p}_\gamma - \vec{p}_{\gamma'}) \Leftrightarrow$$

$$\Leftrightarrow p_{e'}{}^2 = p_\gamma{}^2 + p_{\gamma'}{}^2 - 2 p_\gamma p_{\gamma'} \cos\theta$$

Multiplying both sides by c^2 we can write the previous equation in the form

$$p_{e'}{}^2 c^2 = P_\gamma{}^2 c^2 + p_{\gamma'}{}^2 c^2 - 2 c^2 p_\gamma p_{\gamma'} \cos\theta =$$

$$= (hf)^2 + (hf')^2 - 2(hf)(hf')\cos\theta \quad (2)$$

Recalling the earlier expression (1) for the same quantity, we can equate the two to obtain

$$(hf - hf' + m_e c^2)^2 - m_e{}^2 c^4 = (hf)^2 + (hf')^2 - 2h^2 ff' \cos\theta \Leftrightarrow$$

$$\Leftrightarrow 2h f m_e c^2 - 2h f' m_e c^2 = 2h^2 ff' (1 - \cos\theta)$$

Finally, dividing both sides by $2hff' m_e c$ and considering that $\lambda = \frac{c}{f}$,

$$\frac{c}{f'} - \frac{c}{f} = \frac{h}{m_e c}(1 - \cos\theta) \Leftrightarrow$$

$$\Leftrightarrow \lambda' - \lambda = \frac{h}{m_e c}(1 - \cos\theta)$$

This was the expression first obtained by Compton, although the method he used in his paper for Physical Review in 1923 to derive the equation was not the same as the one exposed here.

The Compton effect has many applications in various fields of natural sciences but, in astrophysics, it is particularly interesting due to its inverse process, the inverse Compton scattering. This process is basically the reverse of the process detailed above, with lower energy photons being scattered to higher energy by relativistic electrons in, for example, the corona of the accretion disk surrounding a black hole.

1.4.2- Bremsstrahlung

A charged particle under acceleration radiates photons. The power for the radiation of a particle q with acceleration *a* is given by Larmor's formula,

$$P = \frac{2q^2 a^2}{3c^3}$$

Hence, the emitted power of this radiation is proportional to the square of both the charge and acceleration.

The photons emitted are in dipolar form, with $P \propto sen^2\theta$, where θ is the angle between the direction of the acceleration and the emission, which leads to the total

absence of emission along the acceleration vector and maximum emission in the direction perpendicular to it (figure 6). The radiation is polarized with the electric field vector of the emitted radiation parallel to the acceleration of the charge.

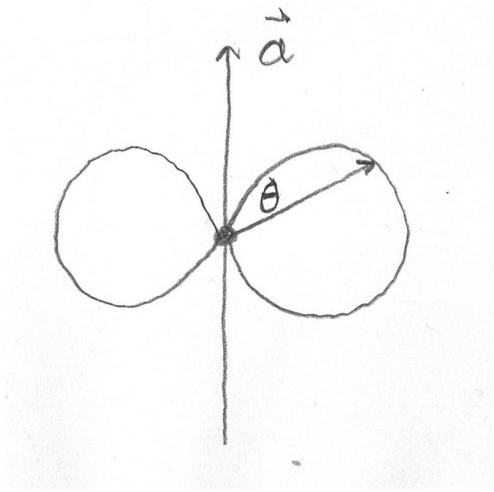

Fig. 7: Dipolar emission from an accelerated charge. Maximum emission occurs when the angle to the acceleration vector is 90º.

Bremsstrahlung, or braking/deceleration radiation, is emitted by a charged particle moving through an electric field $\vec{E}$. The particle emits radiation at the expense of kinetic energy, “braking”.

In Astrophysics, the process is most often observed when an electron passes by a charge of protons. The electron accelerates during the interaction and since this acceleration is not uniform, the emission occurs over a range of wavelengths, creating a spectrum (figure 7). The spectrum is flat up until an upper cut-off frequency ω_{cut} , beyond which it falls exponentially, and can be deduced from Larmor's formula, provided the acceleration as a function of time is known.

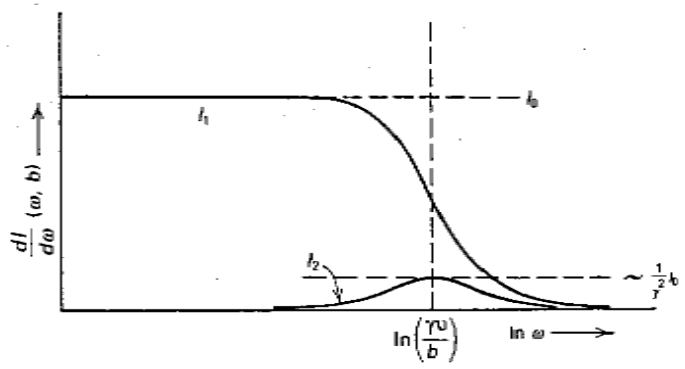

Fig. 8: The spectrum from Bremsstrahlung emission. The point where the spectrum ceases to be flat and starts to fall exponentially is related to the cut-off frequency . This is a diagram for optically thin gases. In case of an optically thick gas, the spectrum would suffer another fall at lower frequencies due to self-absortion. Source: M. S. Longair, High Energy Astrophysics, Vol. I, Cambridge University Press.

The intensity I the flat section of the spectrum is given by,

$$I = \frac{8 Z^2 e^6}{3 \pi c^3 m_e^{\ 2} v^2 b^2} \quad (3)$$

where *b* is the impact parameter for the interaction, i.e. the distance of closest approach, *v* is the velocity of the charge, and *Z* is the number of protons.

Of course, this result is only valid for a single charged particle. If we want to know the emission for a population of electrons, with a given velocity and density dispersion, it becomes necessary to integrate equation (3).

If one considers a cloud of ionized gas with a uniform temperature T, the velocity dispersion is given by the Maxwell distribution:

$$f(v) = 4\pi \left(\frac{m_e}{2\pi kT}\right)^{-\frac{3}{2}} v^2 e^{-\left(\frac{m_e v^2}{2kT}\right)}$$

The parameter *b* is set by the number density of electrons, n_e , and ions, n_i , so, integrating (3) over *v* and *b*, we get the total emitted power per unit volume,

$$e_{ff} = g_{ff} \frac{2^5 \pi e^6}{2 m_e c^2} \left(\frac{2\pi}{2 m_e k}\right)^{-\frac{1}{2}} T^{-\frac{1}{2}} Z^2 n_e n_i e^{-\frac{h\nu}{kT}}$$

where g_{ff} is the gaunt factor, which is of order unity for a wide range of temperatures and density conditions. The subscript "ff" refers to "free-free", alluding to the fact that the electrons and protons move freely during the interaction.

This is the Thermal Bremstrahlung. The spectrum cuts off in *v* at approximately $\frac{h\nu}{kT}$, so the cut-off is a good way of determining the temperature of an ionized HII gas cloud, for example, or the ionized matter in the accretion hole of a black hole.

1.4.3 - Synchrotron Radiation

The fundamental principle behind this process is similar to the one of Bremsstrahlung radiation: a charged particle moving through a magnetic field, radiates energy. At relativistic velocities this phenomenon is known as Synchrotron Radiation.

The relativistic equation of motion for a particle in a magnetic field is,

$$\frac{d}{dt}(\gamma m \vec{v}) = \frac{q}{c} \vec{v} \times \vec{B}$$

where, $\vec{v}$ is the velocity of the charge *q*, m is the mass, γ is the Lorentz factor and $\vec{B}$ is the magnetic field vector.

The motion of the particle is perpendicular to the force acting upon it, so $|\vec{v}|$ remains constant. The direction of the movement, however, can change. If we separate the velocity vector in its components parallel, $v_{\parallel}$, and perpendicular, $v_{\perp}$, to $\vec{B}$, then

$$\frac{d\vec{v}_{\|}}{dt}=0$$

$$\frac{d\vec{v}_{\perp}}{dt}=\frac{q}{\gamma mc}\vec{v}_{\perp}\times\vec{B}$$

The motion is uniform and circular and, if $v_{\|}\neq 0$, the particle spirals along the field lines of the magnetic field. This is what happens on black holes' relativistic jets.

The total power emitted in this case is given by the relativistic equivalent to Larmor's formula:

$$P_{rel}=\frac{2q^2}{3c^3}\gamma^4 a^2$$

The power emitted by a particle under acceleration has a two-lobe distribution around the vector for acceleration. The power depends on the angle relative to the acceleration by

$$P=P_0\cos\theta$$

Synchrotron radiation suffers strong beaming along the direction of motion (figure 8).

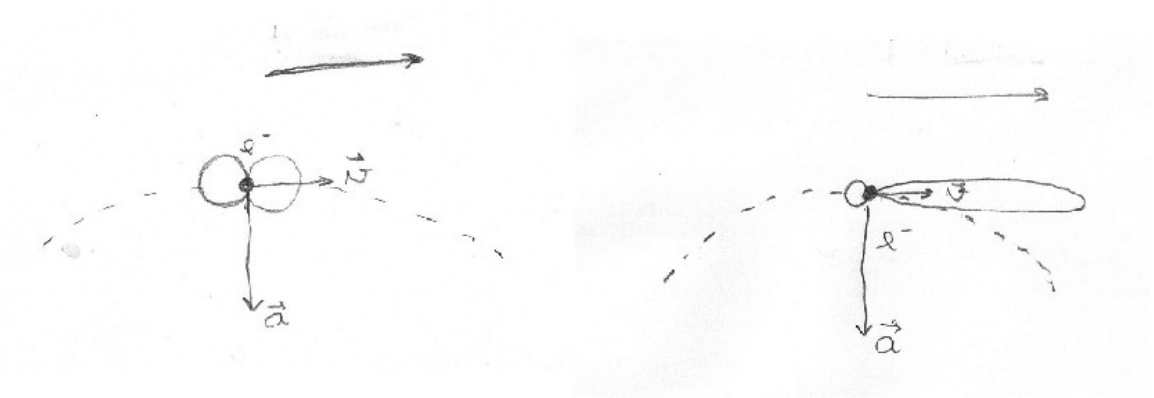

Fig. 9: The effects of beaming on the Synchrotron radiation. On the left the schematic of the radiation of a Cyclotron (the classical equivalent to Synchrotron). On the right the Synchrotron radiation subjected to beaming. The arrows above the schematics indicate the direction to the observer.

This beaming as an effect on the radiation observed: any emission directed to the observer is only detected when the beam is aligned with the observer, originating a flash of radiation with a period much smaller than the gyration period. For the synchrotron, this emission has a characteristic frequency of

$$\nu_c = \frac{3\gamma\omega_B}{2} = \frac{3\gamma^2 eB}{2m_e c}$$

where $\omega_B = \frac{eB}{\gamma m_e c}$ is the frequency of gyration.

The overall spectrum is relatively peaked, with a maximum emission at $\nu_{peak} = 0.29\nu_c$. The frequency at which the peak is reached depends on the intensity of the magnetic field and the mass of the charged particles.

1.5 - The X-ray/Radio Correlation

There are various works regarding the correlations between luminosities at different wavelengths for star forming galaxies and active galactic nuclei (Fabbiano et al. (1984) investigated the relationship between X-ray and Radio/Optical luminosities in a sample of spiral galaxies close to our own first). Here we present some of the most recent ones and try to impress how the correlation may give clues in regards to what happens in the galaxies it is observed in.

Studies of correlations between the x-rays and radio or infrared luminosities for galaxies were responsible for the identification of the X-ray emission as a tracer for star formation in normal galaxies, i.e. non active galaxies (Grimm et al. 2003; Ranalli et al. 2003). Absorption along the X-ray band is rare in galaxies, so these wavelengths are not very sensitive to extinction effects, making X-rays an unbiased indicator for star formation, when it comes to absorption. Since, in star forming, non-active galaxies, the emission in both x-ray and radio bands is, as presented in the previous sections, due to the evolutionary processes of massive stars (the High Mass X-ray Binaries) and their

destruction (electrons accelerated by supernovae), it was suspected that there could be a link between massive stars and the star formation rate.

At high fluxes ($10^{-15} erg\, cm^{-2} s^{-1}$ and higher) most X-ray sources are considered to be active galactic nuclei (Bauer et al. 2000, Lehmann et al. 2001) but, at lower fluxes, appear galaxies which do not fit the AGN category.

Trying to expand on previously existing works, Bauer et al. (2002) made use of the CHANDRA Deep Field North Survey and discovered that there is a good correlation between X-ray and radio luminosity densities for the Survey's Emission-Line Galaxies and nearby late-type galaxies (figure 10), even at moderate redshifts, while pointing the usefulness of X-ray emissions as a tool for the estimation of SFR.

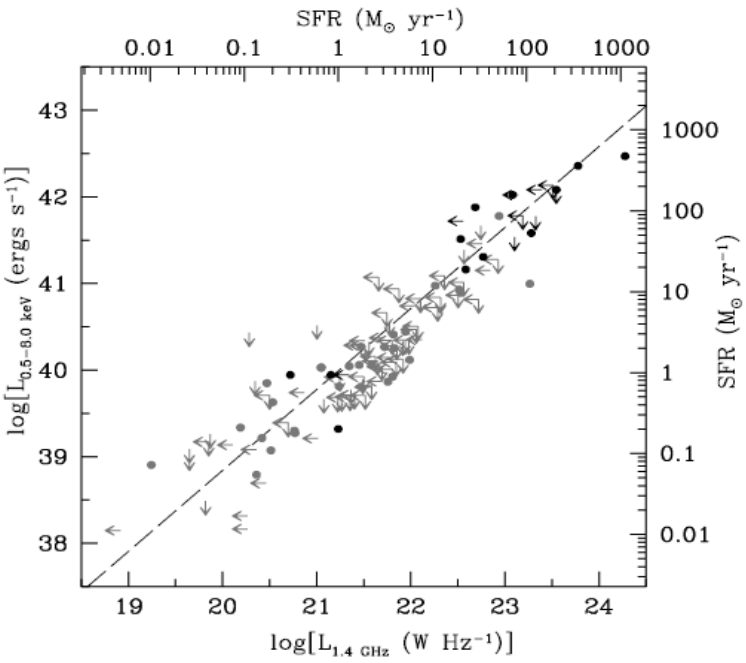

Fig. 10: The correlation between the full band x-ray luminosity and 1.4 GHz radio luminosity for 20 ELG and 102 nearby late-type galaxies, with the respective star formation rates estimated for the sources. From Bauer et al. (2002)

Vattakunnel et al. (2012), on the other hand, used the Chandra X-ray data in conjunction with the deep VLA radio data in the Extended Chandra Deep Field South region and found more than 200 sources detected both in the X-ray and radio bands. From this work resulted the discovery of a correlation between radio and x-ray luminosities for

star forming galaxies up to z~1.5, consistent with the results obtained locally and with no evolution detected in that redshift range (figure 11).

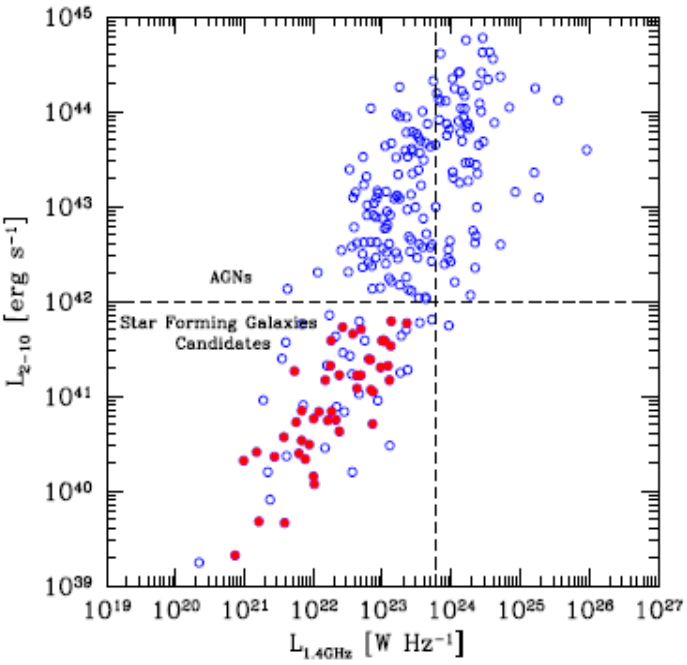

Fig. 11: The correlation for 257 sources detected in both radio and X-ray with measured redshifts. The bottom left square formed by the dashed lines represents the area for Star Forming candidates. Sources above the luminosity values limited by these lines are classified as AGN. However, the lower left corner is merely the candidates for SF and is most likely populated by low luminosity AGN as well. Source: Vattakunnel et al. (2012)

The correlation between X-ray and radio emissions is also extended to Active Galactic Nuclei, as might be apparent by the work done by Vattakunnel et al. (2012). However, when it comes to this point, the matter becomes more complicated as the slope of the correlation, when applied to galaxies possessing AGN, seem to vary depending on whether the galaxies are radio-loud or radio-quiet.

Ballo, L. et al. (2012), analyzed the X-ray, optical and Radio proprieties of AGN and Quasars up to z>2 and discovered that radio-loud AGN also had high emission in the X-ray band and concluded that most of the radio emission for AGN has its origins in the accretion disk (with the exception of beamed sources) and was heavily linked to X-ray

emission. This seems to point to a relation between the correlation and the processes of accretion in the central black holes of a galaxy (Yi, Insu and Boughn, Stephen; 1999, maintain that advection-dominated accretion flow models predict specific correlations for the x-ray/radio luminosities and that a study of these correlations may help confirm and identify galaxies where this particular accretion process takes place).

But the work that illustrates the problem presented above was done by Brinkmann, W. et al. (2000), who studied the correlation for the ROSAT All-Sky Survey from the April 1997 VLA 20cm FIRST catalog, finding that the majority of the sources having an optical counterpart. The correlation derived was found to have different slopes for radio-quiet and radio-loud objects (figure 12).

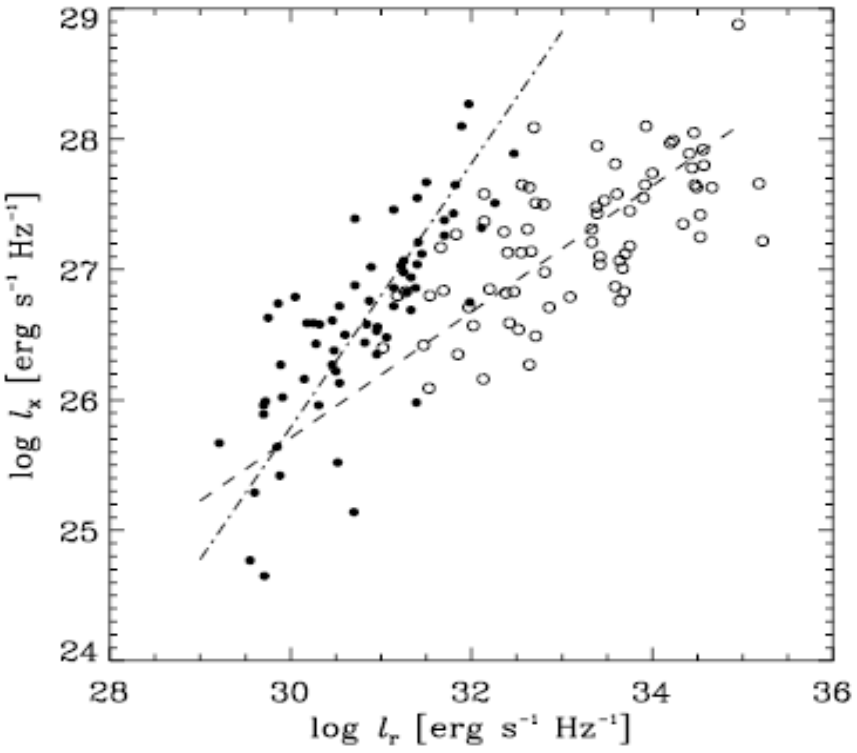

Fig. 12: The correlation between radio and x-ray emissions for the ROSAT All-Sky Survey. The filled dots represent radio-quiet objects and open dots represent radio-loud objects. The dashed and dash-dotted regression lines are for radio-quiet and radio-loud sources, respectively. Source: Brinkmann, W. et al. (2000)

The distinction between the slopes for radio-quiet and radio-loud objects in the correlation may be interesting, since it may help shed some light on the subject of

whether or not there truly is a separation between radio-loud and radio-quiet AGN. Several existing studies seem to consider that the distinction may not even exist, as distributions of the sources do not seem to show obvious bimodal characteristics (Ballo, L. et al. (2012), Brinkmann, W. et al. (2000)).

1.5.1– The Radio and X-ray Emission from Bulgeless Galaxies

Given what has been said until now regarding both bulgeless galaxies and the Radio/X-ray correlation, it is easy to see how the study of the correlation for this type of galaxy may help in their understanding. Comparing the correlation obtained for these objects with the ones existing for other galaxies, it is possible to get clues regarding the evolution these galaxies undergo. Considering that bulgeless galaxies are late-type galaxies (a designation which includes all spiral and irregular galaxies), one would expect the correlation to present similarities to the ones discovered for star forming galaxies (see Bauer et al, 2002, for an example of such correlation). Given that bulgeless galaxies must not have gone through major mergers (because these events would result in the formation of a classical bulge component), it is unlikely for them to possess fully developed AGN's (although there have been examples of these galaxies where the galactic nucleus was active) and so the correlation, if it exists, should follow a slope characteristic of star formation is processes.

The objective of the work presented in this dissertation is inserted in the effort done by the work group at CAAUL dedicated to the study of the problem of bulgeless galaxies (project PTDC/CTE-AST/105287/2008 – The Bulgeless Side of Galaxy Evolution) and consists in trying to determine whether the X-ray/Radio correlation exists for bulgeless galaxies and, if possible, ascertain whether it is indeed more similar to the one observed in star forming galaxies or not. Should the correlation not follow the slope for star forming galaxies, it could mean that these objects possess hidden AGN, not easily detected by regular means, which given what was stated before, would throw our understanding of bulgeless galaxies into disarray.

2. The X-ray-Radio correlation for bulgeless galaxies

2.1 – The COSMOS field

The study of bulgeless galaxies needs the best possible multiwavelength coverage. Research of the evolution of galaxies requires observations across multiple bands, from radio to infrared and optical, all the way to x-rays. Although the number of surveys that meet this requirement is small, there is one which is of particular interest to us: the Cosmic Evolution Survey (COSMOS – Scoville et al. 2007).

The COSMOS survey is a survey that encompasses a large enough area to address the joint evolution of large-scale structure, galaxies, star formation and AGN. It is the largest Hubble Space Telescope (HST) survey undertaken, with an area of approximately two square degrees and located near the equator (RA=10:00:28.6 and DEC=+02:12:21.0). The initial survey was made with the Advanced Camera for Surveys (ACS) and was later expanded with deep multi-wavelength coverage overlapping this area (Koekemoer et al. 2007 – figure 13). This was facilitated by the fact that, being close to the equator, the field used for the COSMOS survey is accessible to a variety of different astronomical facilities. The allocations on Subaru, CFHT and NOAO provided extremely deep photometry for 12 bands from U to K_s allowing for accurate photometric redshifts, integrated colors and color selection of populations (LBGs, AGNs, etc) for the entirety of the objects detected in the 2 deg^2 ACS field. XMM-Newton devoted 1.4Ms for an X-ray survey of the field (Hasinger et al. 2007) and GALEX devoted a deep field survey in the UV band (Zamojski et al. 2007).

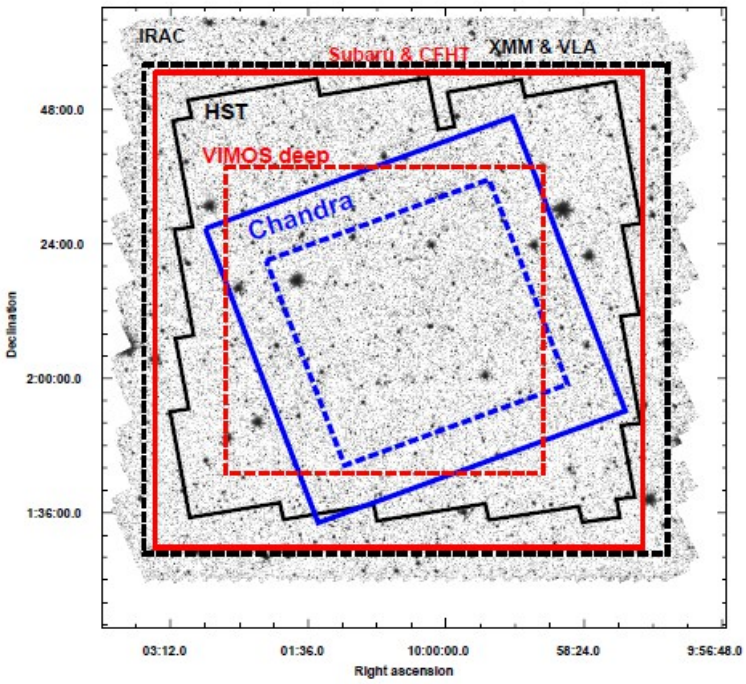

Fig. 13: The area studied by the COSMOS survey, depicting the different areas of coverage of the various multi-wavelength surveys undertaken for the project. The black dashed square details the coverage of both XMM and VLA observatories. The red square refers to the area of the Subaru and CFHT surveys, while the space enveloped by the black, continuous line represents the sky captured by the Hubble Space Telescope. The red dashed square pertains the VIMOS deep survey, the blue square the area covered by the Chandra Large Survey and the blue dashed square the coverage by the Chandra Deep Survey. The background image is the IRAC 3.6μm mosaic. Source: Elvis, Martin, et al. (2009) - The Chandra COSMOS Survey. I. Overview and Point Source Catalog.

Still in the subject of X-rays there was also the Chandra C-COSMOS survey and for the radio band the VLA was used for the survey (more details on these two last surveys can be found on their respective sections, since they were the ones used in this work).

2.2 – The Bulgeless galaxy sample

The high resolution of the Hubble Space Telescope images allow for morphological classification to be made out to high redshifts for the first time, something that Bizzochi et al. (2013) took advantage of by using the morphological catalogue from Griffith et al. (2012) as a base in order to select a sample of bulgeless galaxies selected from four multi-wavelength datasets: COSMOS, AEGIS, GEMS and GOODS. The selections were made at intermediate redshifts – 0.4<z<1.0 – and the rest-frame photometric quantities were derived using $K_{CORRECT}$. The morphological classification was derived from the analysis of the surface brightness obtained at the reddest filter available for each field (I_{F814W} for the COSMOS and EGS fields, z_{F850LP} for the GEMS+GOODS-S fields and i_{F775W} for the GOODS-N field).

The light distribution of the galaxies was analyzed through the fitting of a Sérsic profile:

$$\sum(r) \propto e^{-k\left(\frac{r}{r_e}\right)^{-\frac{1}{n}}-1}$$

where the Sérsic index n describes the shape of the light profile, r_e is the effective radius of the galaxy and k is a positive parameter coupled to n, such that half of the total flux is always within r_e. Figure 14 illustrates the shape of a Sérsic profile for n=1 and n=4. An index of n=1 relates to the exponential profile of a pure-disk galaxy, while n=4 corresponds to the de Vancouleurs' profile of elliptical or spheroid galaxies (Bizzochi et al. 2013).

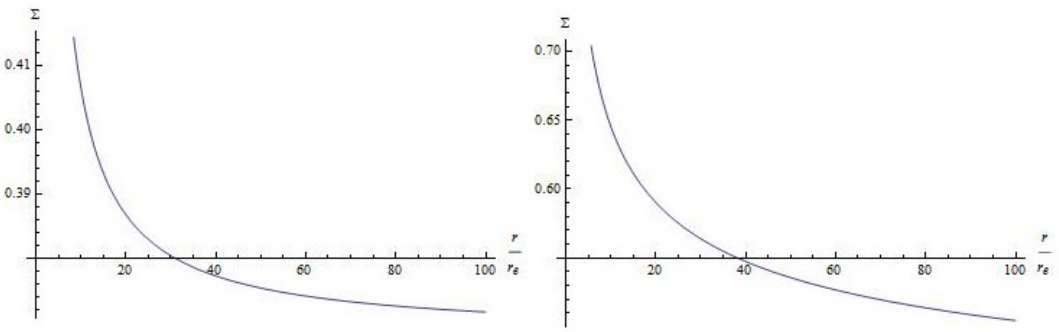

Fig. 14: The Sérsic profiles for n=1 (left) and n=4 (right). An inspection of the plots reveals that the lower the value of n, the sharper the curve becomes. n=1 relates to the exponential profile of a disk galaxy, while n=4 relates to the de Vancouleurs' profile of elliptical galaxies.

For the selection of the final galaxies, the point sources were removed in order to avoid sources without notable morphological information. Likewise, edge-on galaxies were also discarded in order to minimize the effects of dust extinction on galaxy colors and finally, to improve the robustness of the morphology selection, the faintest galaxies were also rejected by imposing a magnitude cut, $m \leq 24$, in the filter considered for each field.

The final selection resulted in 19223 galaxies situated at redshifts between z=0.4 and z=1.0. When possible, the redshifts used in the sample were spectroscopic in nature, with photometric redshifts only being used in cases where reliable spectroscopic redshifts could not be obtained. These redshifts were then used in this project for the estimation of the luminosities for both the Chandra (X-ray band) and VLA (Radio band) selected sources (as detailed in section 2.3).

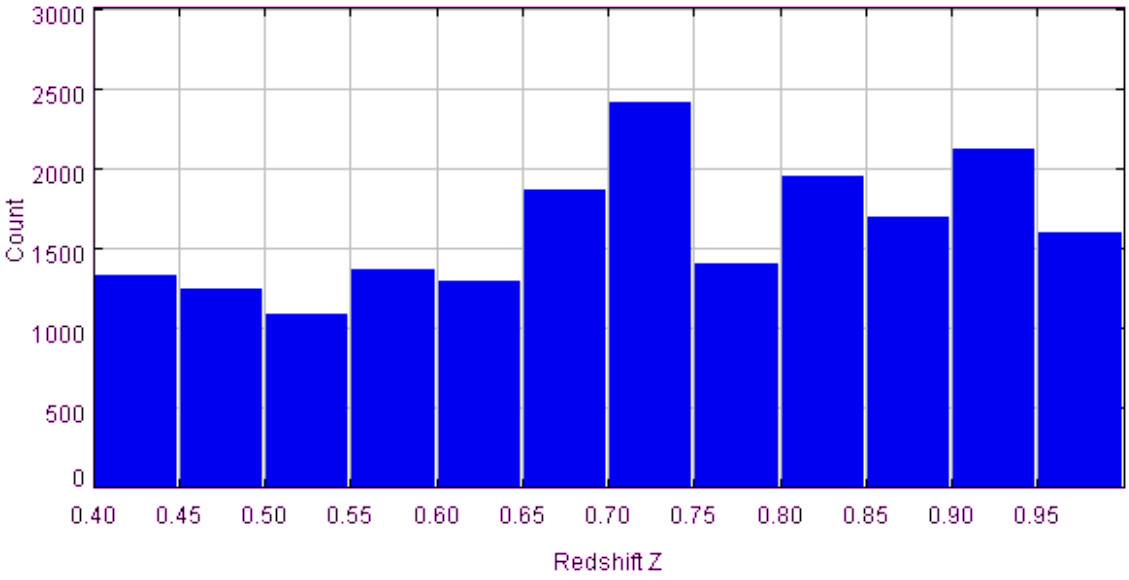

Fig. 15: Redshift distribution for the bulgeless galaxies selection made by Bizzochi et al. (2013). The selection was made for redshifts spanning 0.4<= z <=1.0.

As Figure 15 shows, the sources appear to be relatively even in distribution, when it comes to redshift - although the majority of these sources can be found at redshifts of z=0.6 and greater.

2.2.1 – The X-ray data

In order to identify the sources from the bulgeless catalog that possessed emission in the X-ray band, the catalog by Bizzochi et al. (2013) was correlated with the C-COSMOS survey from the Chandra observatory.

The C-COSMOS survey is a 1.8Ms Chandra program that covers the central contiguous area of approximately 0.92 deg^2 of the COSMOS field. The survey was made in the 0.5 – 10keV band, with a detection limit at $5.7\times10^{-16}\ erg\ cm^{-2}\ s^{-1}$ and resulted in a total of 1761 detected galaxies (bulgeless and otherwise).

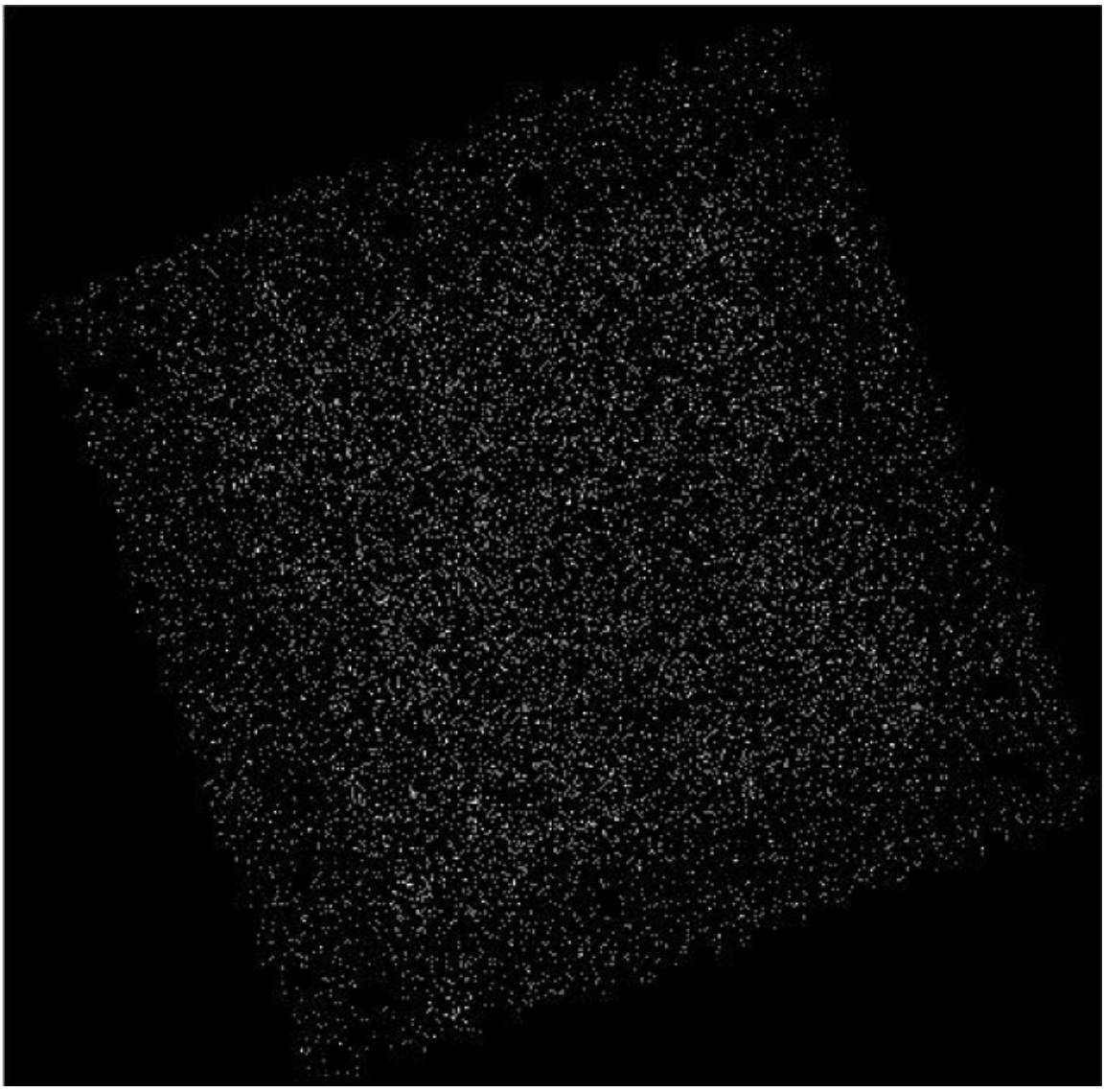

Ilustração 16: The C-COSMOS field as obtained by the Chandra observatory.

These sources were then correlated with the bulgeless galaxies catalog with a tolerance of 6 arc-seconds between the objects' coordinates in both catalogues, in order to account for possible positional errors due to both pointings and detection algorithms. The bulgeless catalog was, has has already been stated, based on a pre-existing one by Griffith et al. (2012) and it retained all the galaxies of that catalog while adding the morphological classification. By correlating the C-COSMOS survey catalog with the bulgeless one, it was possible to see which galaxies had detectable X-ray emission regardless of whether they had bulge or not. This contains resulted in a total of 510 sources detected in the X-ray band. By using the morphological classification added by Bizzochi et al. (2013), it was possible to identify which of those galaxies had no bulge, resulting in 57 galaxies classified as bulgeless, approximately 0.3% of the total bulgeless galaxy sample.

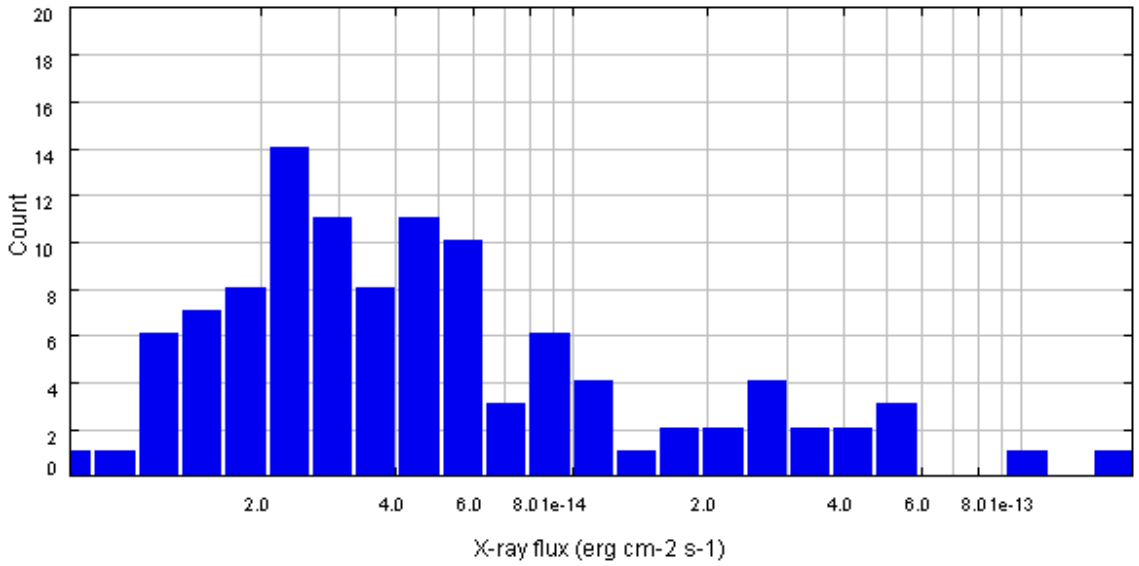

Fig. 17: Flux distribution for the bulgeless galaxies detected in the X-ray band. The axis for the flux (x axis) is set to a logarithmic scale.

Most of the galaxies have a flux of less than $1.0\times10^{-13} erg\ \ cm^{-2}\ s^{-1}$, with the number of sources with emission greater than this limit being almost negligible compared to the whole selected sample (see figure 17).

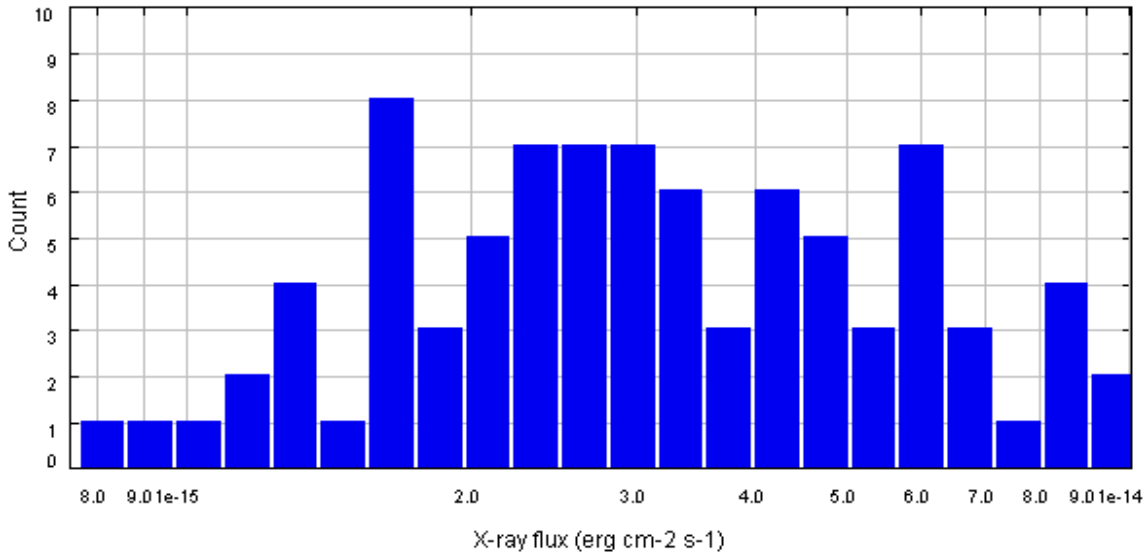

Fig. 18: A more detailed view of the X-ray flux distribution for the bulgeless sample detected with the C-COSMOS survey. Once again the x-axis is in a logarithmic scale.

Moreover, as Figure 18 shows, the majority of the sources are found in fluxes of less than $5.0\times10^{-15}\ erg\ cm^{-2}\ s^{-1}$. The smaller amount of sources with fluxes equal, or superior, to $1.0\times10^{-14}\ erg\ cm^{-2}\ s^{-1}$ seems to suggest that most of the sources in the bulgeless galaxy selection do not possess active galactic nuclei (since AGN are found to have fluxes that are, typically, higher than this value). This is not to say that there can not be AGN with lower fluxes but, in the X-ray band, the amount of AGN detected starts to be overthrown by star forming galaxies when the fluxes fall bellow 10^{-14} erg cm^{-2} s^{-1} (Mushotzky, R., 2004), making it difficult to discern which sources are AGN and which are contaminated by other emission sources. In order to make an informed decision, we need to determine the X-ray luminosities of the galaxies.

2.2.2 – X-ray Luminosities

In order to test whether the coveted radio/X-ray correlation may or may not be present for bulgeless galaxies, it is necessary to turn the radio and X-ray fluxes into their respective luminosities. This section aims to explain how to estimate the X-ray luminosities from the fluxes.

All the luminosities were estimated using the redshifts present on the bulgeless catalog.

As a default, the redshifts are spectroscopic in nature except in the cases where they could not be reliably determined. The spectrum of the galaxy is observed, with the emission or absorption lines being identified and their wavelengths measured. These measured wavelengths are then compared with the rest wavelengths and the redshift is determined (equation 4).

$$z = \frac{\lambda_{obs} - \lambda_{emit}}{\lambda_{emit}} \Leftrightarrow \\ \Leftrightarrow 1 + z = \frac{\lambda_{obs}}{\lambda_{emit}} \quad (4)$$

In the instances where the spectroscopic redshift could not be reliably determined, a photometric redshift was employed. Photometric redshifts, also known as “color-redshifts” or “photo-z”, use broad-band photometry to measure the redshifts of galaxies. The light from the galaxy is measured in different spectral bands (labeled u, g, r, I and z in figure 22). Using a template library of various galaxy types, one can then compare the observed colors in each band to the colors that would be produced by each type of galaxy. Since the templates vary in relation to the redshift, when the method works, the closest match will correspond to the template of not only the right galaxy type but also the correct redshift as well.

Given a determined Redshift, we were then able to use it to estimate the luminosity distances necessary to compute the luminosities (refer to Appendix A.1 for a brief exposition on how Redshifts are used to determine luminosity distances).

The estimate of the X-ray luminosities was made using the method outlined by Afonso, J. et al. (2006), using,

$$L_X = 4\pi d_L^{\,2} f_X (1+z)^{\Gamma-2} \quad erg\ s^{-1}$$

where d_L is the luminosity distance, f_X is the X-ray flux in erg cm^{-2} s^{-1}, z is the redshift and Γ is the photon index, assumed here to be 1.4 since not only was that the value used in the C-COSMOS survey for determining the fluxes but also because, given that bulgeless galaxies are not expected to have many AGN, they are likely to be faint sources in this band and a photon index of 1.4 is expected to give reasonable results (Alexander et al.

2003).

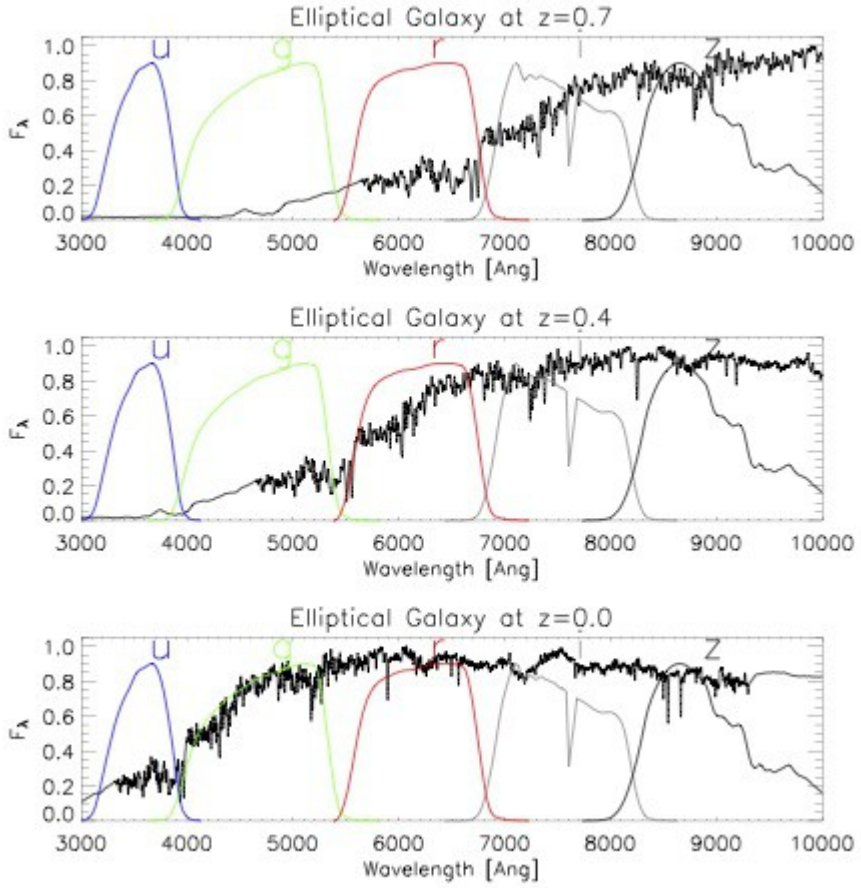

Fig. 19: The spectrum of an elliptical galaxy as it moves through the different photometric bands in relation to the redshift. Different types of galaxy will have different templates. Comparison with templates like this allow for the determination of the redshift of a galaxy. Source: Bruzual and Charlot (2003).

With this, we are now ready to determine the luminosities of the bulgeless galaxies detected in the C-COSMOS survey (X-ray band). But, in order to take some conclusions on the characteristics of the galaxies, we need an additional piece of information: sensitivity limits.

2.2.3 – X-ray Sensitivity limits

One might ask what the interest is in determining the sensitivity limits of the surveys since the only sources that are of interest are those which are, in principle, already detected by the surveys themselves. The answer lies with the fact that knowing these limits lets us have an idea of the validity of the results obtained through the stacking process (section 2.4): since the stacking process is applied only to sources which are not detected in the surveys, in principle the results from the process themselves should be bellow this limit as well. In addition, the knowledge of the sensitivity limits also allows for the estimate of which type of objects to expect (star forming galaxies, AGN, and so on).

Recalling that the detection limit for the C-COSMOS survey is $5.7\times10^{-16}\ erg\ cm^{-2}\ s^{-1}$ erg cm^{-2} s^{-1} and that the bulgeless sources are only considered for a redshift range of $0.4\leq z\leq1.0$ we apply the expression for the X-ray luminosity and are able to obtain an estimate for the luminosity limit for each redshift. Table 1 shows the luminosity limits for redshift intervals of Δz=0.1 for the X-ray band.

Redshift	X-ray Flux (erg cm^{-2} s^{-1})	X-ray Luminosity (erg/s)
0.4	$5.7\times10^{-16}\ erg\ cm^{-2}\ s^{-1}$	3.47649×10^{41}
0.5	$5.7\times10^{-16}\ erg\ cm^{-2}\ s^{-1}$	5.39763×10^{41}
0.6	$5.7\times10^{-16}\ erg\ cm^{-2}\ s^{-1}$	7.78821×10^{41}
0.7	$5.7\times10^{-16}\ erg\ cm^{-2}\ s^{-1}$	1.06576×10^{42}
0.8	$5.7\times10^{-16}\ erg\ cm^{-2}\ s^{-1}$	1.40101×10^{42}
0.9	$5.7\times10^{-16}\ erg\ cm^{-2}\ s^{-1}$	1.78464×10^{42}

Table1: Sensitivity limits for the C-COSMOS Survey. The flux sensitivity of the surveys is the same regardless of the distance of the objects, so the luminosity limit is defined solely by the redshifts.

Depending on the redshift, any galaxy with a luminosity value lower than the limits presented here will not be detected in the X-ray survey.

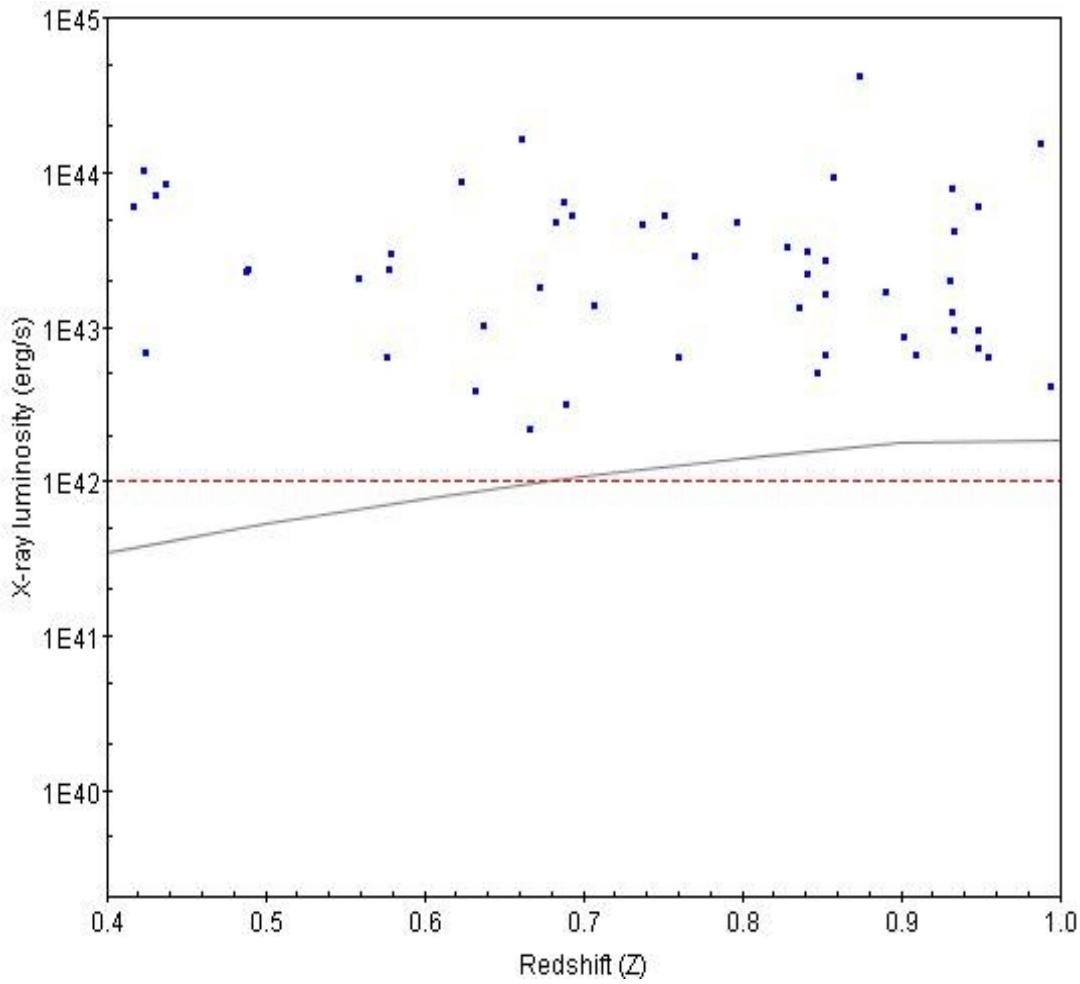

Fig. 20: The bulgeless galaxies detected in the X-ray band by the C-COSMOS survey. The continuous line represents the luminosity detection limit for the survey in respect to the redshift. The dashed line represents the limit above which galaxies are considered AGN.

Figure 23 shows the 57 bulgeless galaxies detected in the X-ray band by the C-COSMOS survey plotted against the line representing the luminosity detection limits of said survey. As expected, all the detected galaxies are above such limits and, indeed, above the limit defined by the luminosity of $10^{42}\ erg\ s^{-1}$, indicating that all the detected sources are AGN.

It's important to remember, though, that the detected sources comprise only 0.3% of the total bulgeless sample, which leaves more than 99% of the bulgeless galaxies out of the X-ray catalog. Not only that, 99% of the bulgeless galaxies are bellow the limit, $10^{42}\ erg\ s^{-1}$ indicating that they are not AGN. But since they are not detected in the survey, our only option is to turn to statistical methods in order to extract the fluxes we need. This process will be covered in section 2.4.

2.2.4 – Radio data

The VLA-COSMOS Large Project imaged the entirety of the 2 deg^2 field encompassed by COSMOS, using the National Radio Astronomy Observatory's (NRAO) Very Large Array (VLA) with a resolution of 1.5'' and a sensitivity of about 11μJy. The original project listed approximately 3600 radio sources; in this work it was used a second, revised edition of the original catalog, limited to sources with a signal to noise ratio greater than 5, resulting in a total of 2617 radio sources.

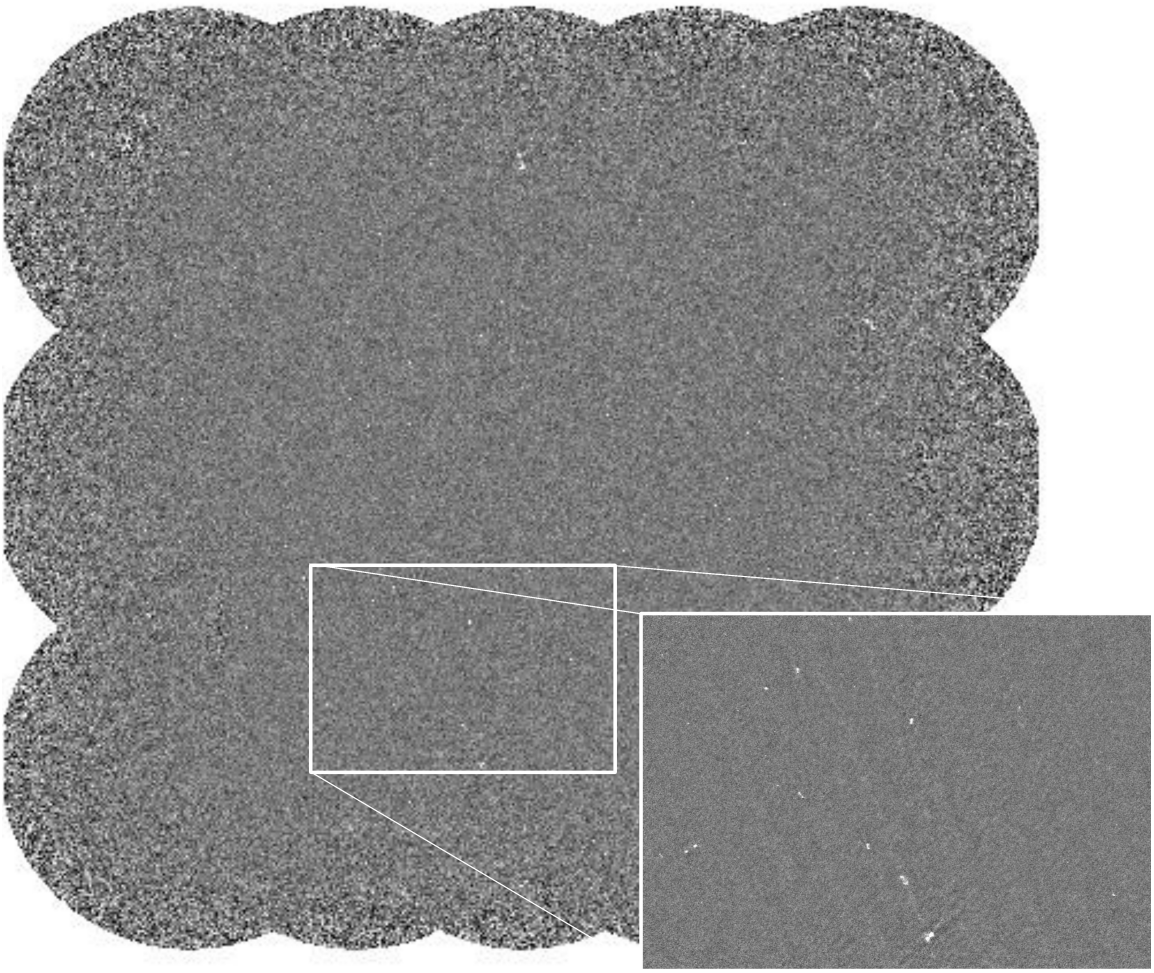

Fig. 21: The VLA-COSMOS Large Project Survey as obtained with the NRAO's VLA. A section of the survey as been zoomed to allow for a better visualization of the sources.

To select the sources in the bulgeless catalog which exhibited radio emission, the catalog from Bizzochi et al. (2013) was correlated with the VLA-COSMOS survey. Keeping in

mind that the catalog is based on the one by Griffith et al. (2012) and that it permits the identification of which of the galaxies present in that catalog are bulgeless, this correlation resulted in the selection of a total of 888 radio-detected sources of which 136 were bulgeless (approximately 0.71% of the total bulgeless galaxy selection). Similarly to the case for X-rays, there was an allowed discrepancy in the comparison of coordinates to a maximum of 6 arc-seconds to allow for the positional errors due to both pointings and detection algorithms.

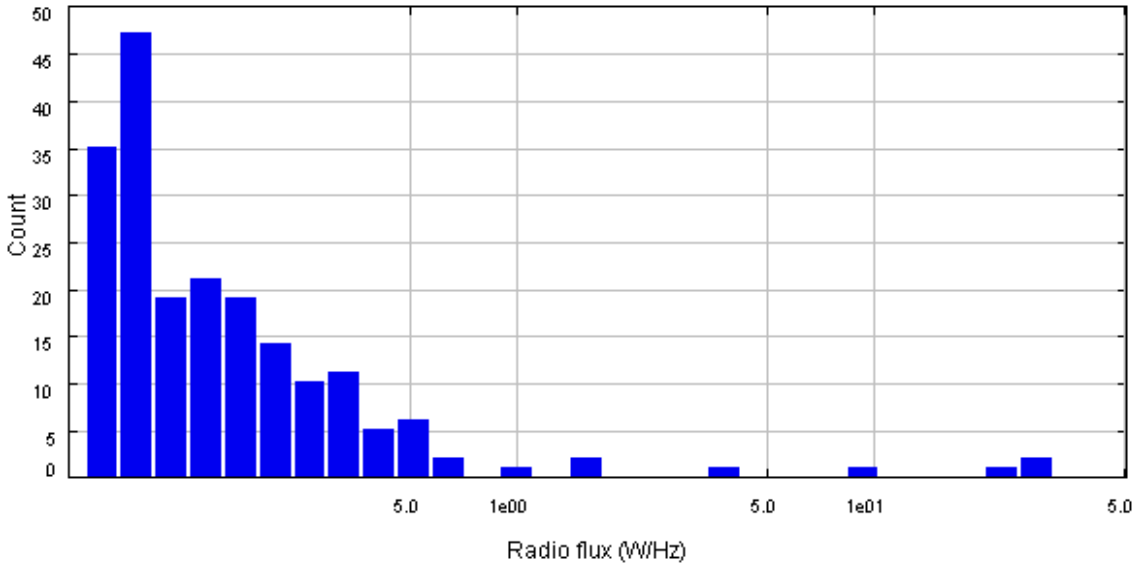

Fig. 22: Flux distribution for the radio-detected sources as captured by the VLA-COSMOS Large Survey. Like in the previous instances, the flux is set to a logarithmic scale and has units of mJy. The majority of the sources can be found at fluxes smaller than 10 mJy.

Most of the objects detected in the survey have fluxes bellow the 10mJy mark (figure 25). The sources whose fluxes go beyond this value are mostly identified as multiple component sources and there are no bulgeless galaxies identified there. A more detailed analysis of the flux distribution shows that the concentration of sources spikes for fluxes bellow 0.2mJy.

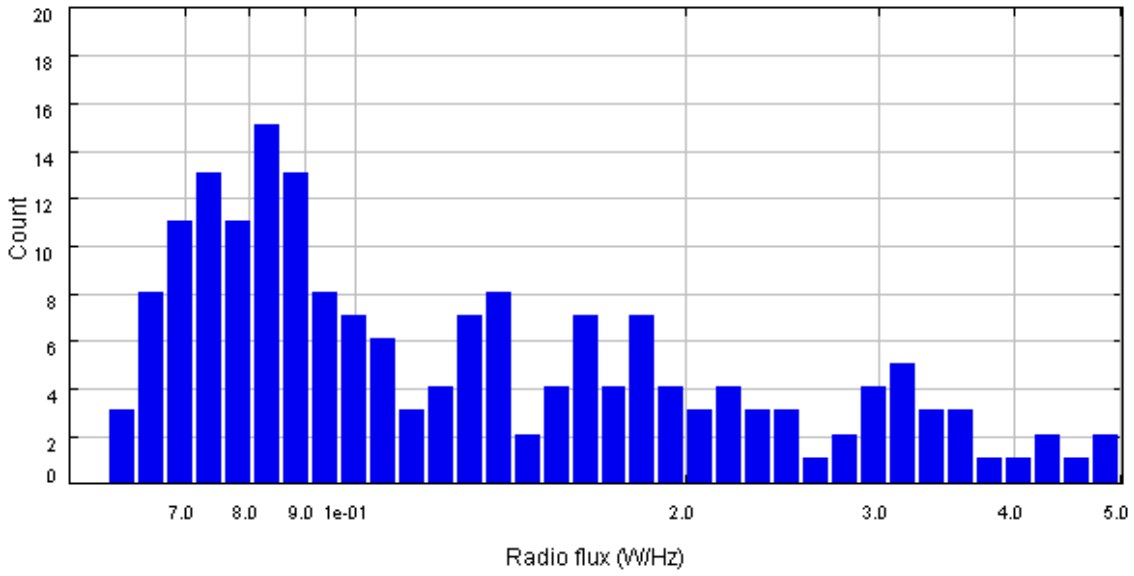

Fig. 23: The flux distribution for the bulgeless sources detected in the VLA-COSMOS Large Survey from 0 to 0.5 mJy. Once again, the flux is set to a logarithmic scale with units of mJy. The detection number seems to be greater for fluxes bellow 0.2 mJy.

Figure 26 shows a new flux distribution of the same sources, this time restricted to a maximum of 0.5 mJy of intensity. Given that, for fluxes above 100 μJy, many radio sources are mostly found to be radio-loud AGN (Ballantyne, D. R., 2009) and that 86% of the total radio-selected bulgeless sample has a flux bellow this value, it may, perhaps, be expected for a good portion of the radio-detected sources to be either star forming galaxies or radio-quiet AGN. To actually be sure, however, we have need, once again, of luminosities.

2.2.5 – Radio Luminosities

In similarity with the case for the X-ray survey, the estimation of the radio luminosity was also made through the process detailed in the previously mentioned paper by taking

$$L_{1.4\mathrm{GHz}} = 4\pi d_L^{\,2} S_{1.4\mathrm{GHz}} 10^{-33} (1+z)^{\alpha-1} \quad WHz^{-1}$$

where d_L is, once again, the luminosity distance, $S_{1.4\mathrm{GHz}}$ is the flux density in mJy and α is

the radio spectral index (assumed to be 0.8, the characteristic spectral index of synchrotron radiation – one of the major sources of radio emission in both AGN and Star Forming Galaxies). As before, in the estimation of the distances, spectroscopic redshifts were preferred, with photometric redshifts being used only when the firsts were not available. And as before, we can take some conclusions in regards to the bulgeless galaxies

The VLA-COSMOS survey as the average sensitivity of 10.5 mJy. Using this value as flux and applying the expression from Afonso et al. (2006), it is possible to estimate the luminosity from such flux for a variety of redshifts. Once again, since the bulgeless sources only go from z=0.4 to z=1.0, the sensitivity estimates were made for this range of values (considering only the lower redshifts), in intervals of Δz=0.1.

Redshift	Radio Flux (μJy)	Radio Luminosity (W/Hz)
0.4	10.5	7.32667×10^{21}
0.5	10.5	1.16937×10^{22}
0.6	10.5	1.73141×10^{22}
0.7	10.5	2.42747×10^{22}
0.8	10.5	3.26487×10^{22}
0.9	10.5	4.24977×10^{22}

Table 2: Sensitivity limits for both C-COSMOS and VLA-COSMOS surveys. The flux sensitivity of the surveys is the same regardless of the distance of the objects, so the luminosity limit is defined solely by the redshifts.

As with the case for the X-rays, all galaxies with radio luminosities bellow these values (with corresponding Redshifts) will not be detected by the VLA-COSMOS survey.

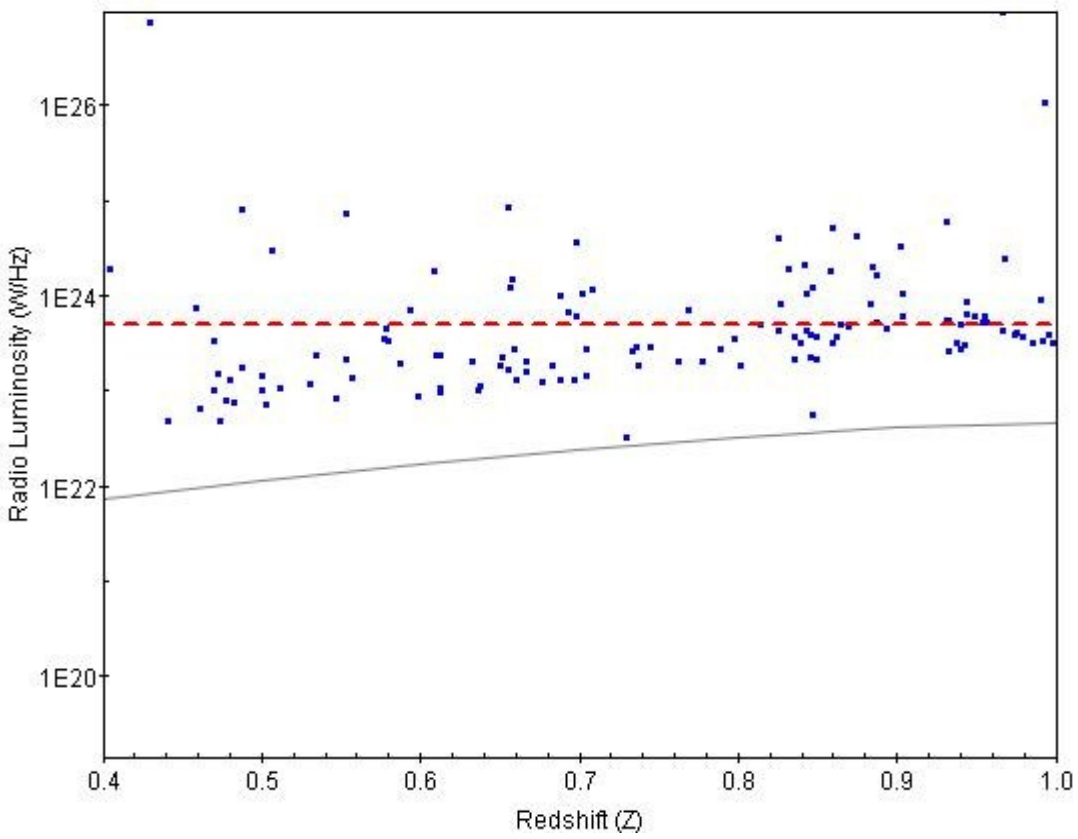

Fig. 24: The bulgeless galaxies detected in the Radio band by the VLA-COSMOS Large survey. The continuous line represents the luminosity detection limit for the survey in respect to the redshift. The dashed line represents the limit above which galaxies are considered AGN.

An inspection of figure 27 reveals a difference when compared with the results obtainned for the X-rays case: although a small number, 48, of the bulgeless galaxies are still above the luminosity limit set for AGN (~10^{23} W/Hz), most of the detected bulgeless galaxies (88 galaxies, approximately 65% of the radio detected total) are bellow this luminosity and are not considered AGN. This equates to about 0.25% of the total bulgeless galaxy sample being classified as AGN based on their radio luminosities, a result that is in concordance with the result obtainned previously for the X-ray band (0.3% of the total population was classified as AGN).

2.3 – The Radio/X-ray Correlation (Detected Sources)

Once the X-ray and Radio sources are selected, all that remains is to see how many of these possess emission on both bands. This was achieved by once again cross-correlating the sources, using the same constraints relayed in sections 2.2.1 and 2.2.4. The result was a total of 18 galaxies.

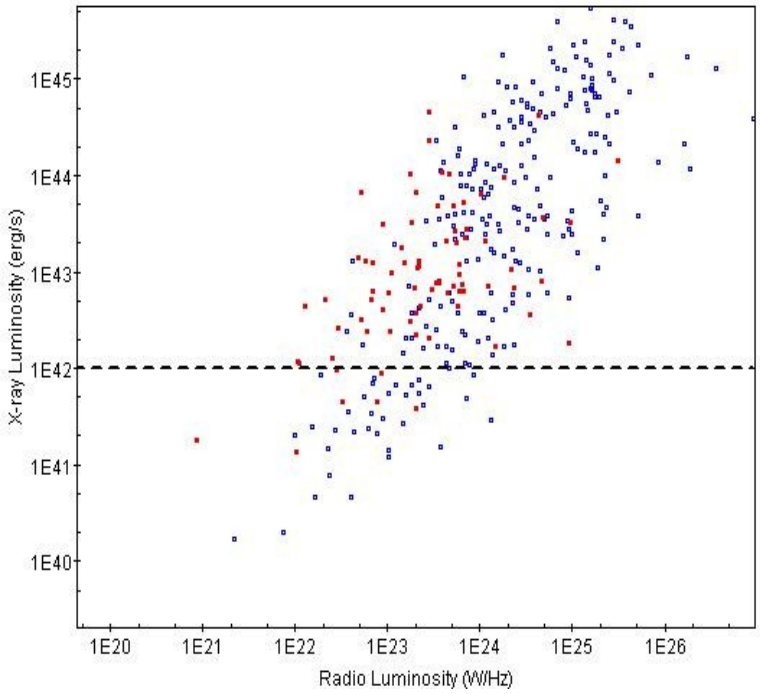

Fig. 25: The correlation between Radio and X-ray luminosities for all the galaxies (bulgeless or not) detected on both C-COSMOS survey (X-rays) and VLA-COSMOS Large survey (radio). The sources were plotted against the correlation obtainned by Vattakunnel et al. (2012) as a means of comparison, revealing that the results obtainned for our sources are in agreement with previous results. The dashed line marks the limit above which sources are considered AGN.

Figure 28 shows the correlation between X-ray and Radio luminosities for the 111 galaxies present in both the C-COSMOS and VLA-COSMOS surveys. On the plot one can see the correlation found by Vattakunnel et al. 2012 in the background of the correlation found in this work, showing that both selection appear to follow a similar correlation. Of the 111 galaxies only 7 are decisively bellow the limit usually used for X-

ray luminosities of AGN, marking them as possible candidates for star forming galaxies (L_X<10^{-42} erg/s). This is not an exact limit, however, since Type-2 AGN (AGN which present only narrow lines in their spectrum, due to obscuration by dust) can also have X-ray luminosities inferior to 10^{-42} erg/s. This concordance with previous works is comforting since, because bulgeless galaxies are included in the sample, it may indicate the presence of the correlation for these types of galaxies.

If one considers only bulgeless galaxies, the sample is considerably diminished, with only 18 galaxies being detected as having both X-ray and Radio emission (figure 29).

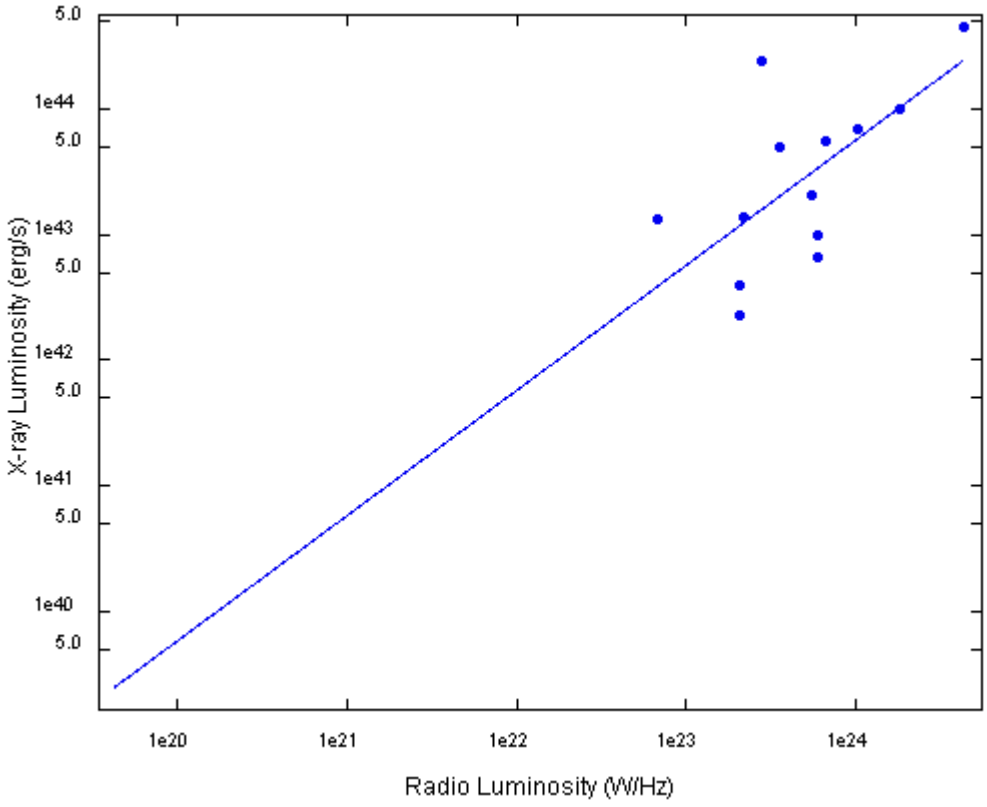

Fig. 26: The X-ray/Radio correlation for bulgeless galaxies only. The line represents the linear regression obtained from the plot-points.

The linear regression obtained shows a correlation of the form $L_{X-ray}=0.998\times L_{radio}+19.77$, which has a slope very similar to the one found in the correlations obtained by Brinkmann et al. (2000) for radio-quiet AGN: $L_{X-ray}=(1.012\pm0.083)L_{radio}+(-4.57\pm2.55)$. This also falls in line with our luminosity analysis and with our comparison with Vattakunnel et al. (2012), since all the sources have X-ray luminosities inferior to 10^{42} erg/s and are classified as active galactic

nuclei.

2.4 – Stacking

As has been stated in sections 2.2.3 and 2.2.5, most of the bulgeless galaxies were not detected either in the radio survey or in the X-ray one. As such, it is impossible to take the fluxes for these sources directly from the catalogs themselves. There is, however, an option and that is the use of stacking techniques.

The main problem when it comes to source detection in any kind of signal is the ratio between the strength of the signal itself and the background noise that is always present. Stacking is a way to overcome this obstacle. When a source is not detected by a given survey, it's either not there or it has a signal that isn't able to stand out from the background noise. But the thing about background noise is that it is, at its core, a random characteristic of images. There are several sources of noise in an image including the noise created by the instruments themselves and the temperature at which the measurements are made. However, the background noise from the sky itself is a statistical quantity that isn't constant. What stacking techniques do then, is to take several different images (either from the same source or from different sources) and add them together. Because of the random, statistical property of the background noise this quantity never rises and, in fact, tends to stabilize at a given value. On the other hand the undetected sources are being added and constantly making the source signal grow – eventually the enough images are added to make the signal-to-noise ratio be high enough that the source can finally be distinguished from the background, enabling us to take, for example, the values for its fluxes.

There have been several works that have made use of stacking techniques to obtain fluxes otherwise impossible to register, particularly in the radio band of the spectrum (Messias et al. 2010), infrared (Zheng et al. 2009, Bourne et al. 2010) and sub-millimeter bands (Martínez-Sansigre et al. 2009) - the very software used in this work was originally conceived as a means to use stacking techniques on the different radio surveys.

In this project, the stacking process was made by adding images of all the sources that

weren't detected in the VLA-COSMOS and C-COSMOS surveys. By providing a list of coordinate sets (R.A. and Dec. in decimal units), the software isolated the positions of the source not detected in the original surveys directly in the full image of both the C-COSMOS and VLA-COSMOS surveys. Although the process went smoothly for most of the sources there were complications with the C-COSMOS part of the coordinate mapping since, given that the coverage area of this survey is smaller than the bulgeless galaxy one, several galaxies would fall outside the range of the survey and had to be disregarded. The stacking itself was made using redshift bins of $\Delta z=0.1$, starting from $z=0.4$ until $z=1.0$ (Table 2), and resulted in six average galaxies obtained from sources not detected in neither the X-ray nor Radio bands.

Redshift Bin	Number of selected galaxies (no X-ray emission)	Number of selected galaxies (no Radio emission)
$0.4 \leq z \leq 0.5$	2356	2551
$0.5 \leq z \leq 0.6$	2359	2403
$0.6 \leq z \leq 0.7$	3010	3108
$0.7 \leq z \leq 0.8$	3605	3747
$0.8 \leq z \leq 0.9$	3249	3582
$0.9 \leq z \leq 1.0$	3155	3687

Table 3: The Redshift bins used in the stacking process for galaxies without X-ray emission and for galaxies without Radio emission, with the respective number of sources detected for each bin.

For the redshift used in the estimation of luminosities for each bin it was decided to merely consider the central values for the redshift bins (i.e. $z=0.45$, $z=0.55$, and so on until, and including $z=0.95$), resulting in an average of about 3200 galaxies per redshift bin being stacked in a single “average” object (as illustrated in figure 30).

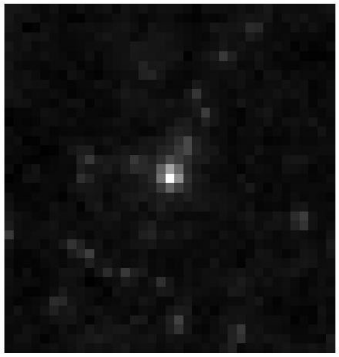

Fig. 27: The result of the stacking of 3582 sources in the radio band at a redshift of z=0.85.

The six average galaxies obtained through this process were then plotted against the galaxies detected in the x-ray and radio surveys in order to see their positions in the correlation. The result of this process is shown in section 2.5.1.

2.4.1 – Undetected sources

So far the results obtained seem fairly concordant with what might be expected given the nature of the sources but how does the correlation change when considering the galaxies which are not detected in the C-COSMOS and VLA-COSMOS surveys (X-ray and Radio bands, respectively)? In fact, the vast majority of the bulgeless galaxies (approximately 19000 galaxies) are not identified in either catalog and it should be interesting to investigate what the correlation is for these objects. The stacking process produced, as has already been stated, a total of six average galaxies from the total bulgeless galaxies without both X-ray and Radio emission (figure 31).

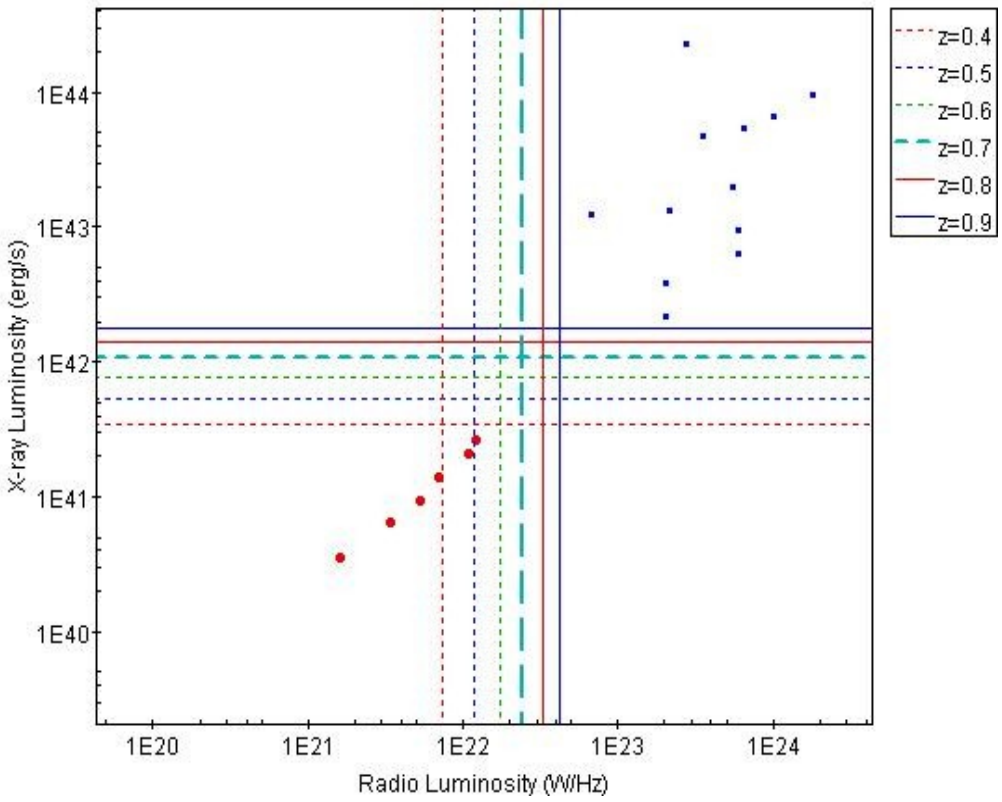

Fig. 28: The "average" galaxies obtained in the stacking process (blue squares). The staking results were plotted against the original correlation as background to provide a clearer representation of the overall position of the sources. The stacked bins' luminosities grow with the redshif: the lower-left source corresponds to the lowest redshift bin while the upper-right refers to the highest redshift bin. The lines represent the luminosity sensitivity limit for the indicated value for Redshift.

The linear regression yields the expression $\log(L_X)=0.9835\times\log(L_R)+20.657$, very similar to the result obtained in the correlation for the COSMOS sources and both the results from Bauer et al. (2002), with a correlation of the form $\log(L_{X-ray})=(0.935\pm0.073)\times\log(L_{radio})+(20.141\pm1.650)$ for star forming galaxies. Even better, since the stacked galaxies comprise approximately 99% of the total bulgeless galaxy population, the fact that their correlation is identical to the ones determined for the general galaxy population (let's not forget that the bulgeless galaxies detected in the X-ray and Radio surveys also followed the correlation for normal galaxies with AGN), this may indicate that the processes responsible for these emissions are the same for both populations, establishing a link between the two tipes of galaxies.

3 – Conclusion and Discussion

Sections 2.3 and 2.4 presented the correlations obtained for both the sources detected in the relevant surveys as well as for the ones subject of stacking process applied to galaxies without X-ray and Radio emission.

The correlation obtained for the first case is indistinguishable from previous correlations obtained in preexisting works for sources classified as Active Galactic Nuclei (Brinkmann et al. 2000 and Vattakunnel et al. 2012). At first glance and considering that bulgeless galaxies are expected to be defined more as star forming galaxies rather than AGN, one might be inclined to dismiss this result as incorrect. However, this is a result that was already somewhat expected, given that the luminosity sensitivity limits for the surveys used favor AGN as sources in detriment of objects with lower emissions such as star forming galaxies. Another compelling clue to the acceptance of this result is the fact that the number of bulgeless galaxies detected in the surveys (18 – 0.01% of the total bulgeless selection) is similar to the total number of AGN identified in the original sample by Bizzochi et al. (2013) – 0.015% of the total number of bulgeless galaxies. If one adds in the fact that the sources are concentrated in luminosity values above the limit of 10^{-42} erg/s for the X-rays, a good sign of the presence of Active Galactic Nuclei, the results appear to be coherent.

As for the bulgeless galaxies not detected in the surveys, the correlation found bears similarities with the ones found by Bauer et al. (2002) for star forming galaxies. This result is encouraging, since, from the beginning, since bulgeless galaxies were expected to owe their emission primarily to star forming related processes. There is however a definite uncertainty related to the definite form of the correlation. This problem arises from the fact that the correlations themselves not yet well understood and the values obtained for them vary according to the methodology used by the author – for example, Vattakunnel et al. (2012) reports different results for the correlation depending on whether the correlation is left to form freely or if it is constrained to a slope of unity. This variability in the results makes taking assured conclusions somewhat difficult.

The results obtained here show that the X-ray/radio correlation is also verified for bulgeless galaxies. Taking into account that bulgeless galaxies do not, in general, show AGN, this result strongly suggests that the correlation exists due to Star Forming processes and not only because of AGN processes as shown in previous works. Further research is necessary not only for the possible confirmation of the results achieved in this project but also in the attempt to further its application. A possible way to do this would be to make use of other surveys, such as the XMM-Newton: because it's area of effect is as large as the COSMOS field – much like VLA-COSMOS is – the number of galaxies that have to be discarded due to not being in the X-ray field is diminished – perhaps even rendered null -, which would yield more galaxies available for both the stacking processes and the detected x-ray bulgeless sample. Since the bulgeless catalog used in this work was created used various different surveys, it would be interesting to see if the correlation could be confirmed for the bulgeless galaxies other than the ones detected in the COSMOS field. It would be also interesting to investigate whether the correlation varies depending on the hardness ratio of the sources. This would allow for the inspection of the correlation for different objects (type-1 AGN, type-2 AGN, QSO's and star forming galaxies) and whether or not there are different correlations for these objects. The same correlation for different objects could imply that the process that give birth to the emission in the X-ray and Radio bands are related for different classes of galaxies and that maybe they share a common evolutionary link. This is something that might even be extended to the question of the separation between radio-quiet and radio-loud AGN. The dichotomy between radio-loud and radio-quiet AGN has been in discussion for some time with some authors defending that it might not be valid at all (Brinkmann et al. 2000). If there is no variation in the correlation for radio-loud and radio-quiet AGN, this might be an indication that maybe there is no clear separation between the two objects...

Appendices

A.1-Distance estimates

The estimate of the luminosity distance is indispensable for the determination of the luminosities.

The luminosity distance d_L is defined by the relation between bolometric (integrated over all frequencies) flux S and bolometric luminosity L:

$$d_L = \sqrt{\frac{L}{4\pi S}}$$

If the concern is not with bolometric quantities but rather with differential fluxes and luminosities, then it is necessary to include a correction, the k-correction, in order to account for the effects of redshift in regards to the difference between the emitted light and the observed one, with the relation between a differential flux S_ν and the differential luminosity L_ν being given by

$$S_\nu = (1+z)\frac{L_{(1+z)\nu}}{L_\nu}\frac{L_\nu}{4\pi {d_L}^2}$$

where z is the redshift, the ratio of luminosities is equal to the difference in flux between observed and emitted bands, and the factor of (1+z) accounts for the redshift in the bandwith (Peebles, 1993, pp. 330-331).

However, although these formula do permit the estimation of the luminosity distance, they are not the indicated ones for the determination of distances on an extra-galactic scale. The formula above are used in the context of distances between stars – for distances between galaxies, particularly distant galaxies, one has to make use of Redshift.

This can be done by considering the fact that the luminosity distance is related to both the comoving distance and the angular diameter distance (Weedman, 1986, pp. 60-62)

by

$$d_L = (1+z)^2 d_A = (1+z) d_M$$

where d_A is the angular diameter distance and d_M is the transverse comoving distance.

The first one, the angular diameter distance, is defined as the ratio of an object's physical transverse size to its angular size (in radians) and is used to convert angular separations in telescope images into proper separations at the source. It is curious in the way that, beyond redshifts of z=1, the more distant objects are, the greater their apparent angular size. Unfortunately, the surveys used do not provide the necessary information required for the estimation of this quantity either and we are forced to turn our focus onto the second option.

The comoving distance between two events at the same redshift but separated on the sky by some angle δθ is $d_M \delta\theta$ and the transverse comoving distance d_M is given by

$$d_M = \begin{cases} D_H \frac{1}{\sqrt{\Omega_k}} \sinh[\sqrt{\Omega_k} d_C / D_H] & for \quad \Omega_k > 0 \\ d_C & for \quad \Omega_k = 0 \\ D_H \frac{1}{\sqrt{\Omega_k}} \sin[\sqrt{\Omega_k} d_C / D_H] & for \quad \Omega_k < 0 \end{cases}$$

where the trigonometric functions account for the curvature of space.

The comoving distance is the equivalent to the proper motion distance defined as the ratio of the actual transverse velocity of an object to its proper motion (in radians unit per time, as defined in Weinberg, 1972, pp. 423-424), and that is the reason for being represented by dM. However, although the luminosities are no longer present, we are now faced with two new quantities that we must explore: d_C and D_H.

DH is simply the Hubble distance, the speed of light times the Hubble time – which is the inverse of the Hubble constant. It is defined as

$$D_H \equiv \frac{c}{H_0}$$

in a cosmology context, these quantities are generally defined as to be equal to unity

($c=t_H=D_H=1$).

As for d_C, it stands for line-of-sight comoving distance and is computed by integrating infinitesimal δd_C contributions nearby events along the radial ray from z=0 to the object. This quantity is obtained by first defining a function

$$E(z)\equiv\sqrt{\Omega_M(1+z)^3+\Omega_k(1+z)^2+\Omega_\Lambda}$$

This function is proportional to the time derivative of the logarithm of the scale factor $(\dot{a}(t)/a(t))$ with z being the redshift and Ω_M, Ω_k and Ω_Λ being the three density parameters (Peebles, 1993, pp.310-321). As $dz=da$, $\frac{dz}{E(z)}$ is proportional to the time-of-flight of a photon travelling across a redshift interval divided by the scale factor. This is the definition of a comoving distance. The total line-of-sight comoving distance is then given by

$$d_C=D_H\int_0^z\frac{dz'}{E(z')}$$

By computing the line-of-sight comoving distance, one can then obtain the transversal comoving distance and use it to achieve the luminosity distance without relying on the fluxes and luminosities. The only things needed are the redshifts, which are provided in the surveys, the Hubble constant and the density parameters – adopted in this work as $H_0=70\ kms^{-1}\ Mpc^{-1}$, $\Omega_M=0.3$, $\Omega_\Lambda=0.7$ and $\Omega_k=0$.

Having a way to estimate the luminosity distances, it is now possible to make some guesses as to what the sensitivity limit should be for both the C-COSMOS and VLA-COSMOS surveys when it comes to luminosities.

References

- Abadi, M. G., et al., Simulations of Galaxy Formation in a Λ Cold Dark Matter Universe. II. The Fine Structure of Simulated Galactic Disks, The Astrophysical Journal, Volume 597, Issue 1, pp. 21-34.
- Afonso, J.; Mobasher, B.; Koekemoer, A.; Norris, R.P.; Cram, L., Optical and X-ray Identification of Faint Radio Souces in the GOODS-S ACS Field, The Astronomical Journal, Volume 131, Issue 3, pp. 1216-1230.
- Arad, I.; Lynden-Bell, D., Inconsistency in theories of violent relaxation, Monthly Notices of the Royal Astronomical Society, Volume 361, Issue 2, pp. 385-395.
- Ballantyne, D., The Contribution of Active Galactic Nuclei to the Microjansky Radio Population, The Astrophysical Journal, Volume 698, Issue 2, pp. 1033-1041 (2009).
- Ballo, L.; Heras, F. J. H.; Barcons, X.; Carrera, F. J., Exploring X-ray and radio emission of type 1 AGN up to z ~ 2.3, Astronomy & Astrophysics, Volume 545, id.A66, 15 pp.
- Bauer, F. E., et al., The Chandra Deep Field North Survey. XII. The Link between Faint X-Ray and Radio Source Populations, The Astronomical Journal, Volume 124, Issue 5, pp. 2351-2363.
- Beckmann, V.; Shrader, C., The AGN phenomenon: open issues,Proceedings of "An INTEGRAL view of the high-energy sky (the first 10 years)" - 9th INTEGRAL Workshop and celebration of the 10th anniversary of the launch (INTEGRAL 2012). 15-19 October 2012. Bibliotheque Nationale de France, Paris, France. Published online at http://pos.sissa.it/cgi-bin/reader/conf.cgi?confid=176, id.69. Also available at http://arxiv.org/abs/1302.1397v1.
- Bell, Eric F., Estimating Star Formation Rates from Infrared and Radio Luminosities: The Origin of the Radio-Infrared Correlation, The Astrophysical Journal, Volume 586, Issue 2, pp. 794-813.
- Benson, A. J., et al, What Shapes the Luminosity Function of Galaxies?, The Astrophysical Journal, Volume 599, Issue 1, pp. 38-49.

- Benson, A. J., Galaxy formation theory, Physics Reports, Volume 495, Issue 2-3, p. 33-86.
- Bourne, N, et al., Herschel-ATLAS: the far-infrared-radio correlation at z < 0.5, Monthly Notices of the Royal Astronomical Society, Volume 409, Issue 1, pp. 92-101.
- Brinkmann, W., et al, Radio and X-ray bright AGN: the ROSAT-FIRST correlation, Astronomy & Astrophysics, Volume 356, pp. 445-462.
- Bromm, Volker; Loeb, Abraham, Formation of the First Supermassive Black Holes, The Astrophysical Journal, Volume 596, Issue 1, pp. 34-46.
- Brook, C. B., et al., The Emergence of the Thick Disk in a Cold Dark Matter Universe,The Astrophysical Journal, Volume 612, Issue 2, pp. 894-899.
- Bruzual G., Charlot S., 2003, MNRAS, 344, 1000
- Buat, V.; Xu, C., Star formation and dust extinction in disk galaxies. Comparison between the UV non-ionizing and the FIR emissions, Astronomy and Astrophysics, v.306, p.61.
- Buckert, Andreas; Tremaine, Scott, A Correlation Between Central Supermassive Black Holes and the Globular Cluster Systems of Early-type Galaxies, The Astrophysical Journal, Volume 720, Issue 1, pp. 516-521 (2010).
- Carlberg, R. G., Galaxy formation and clustering in an N-body experiment, Astrophysical Journal 332, 26-43.
- Ciotti, Lucca; Ostriker, J. P.; Proga, Daniel, Feedback from Central Black Holes in Elliptical Galaxies. I. Models with Either Radiative or Mechanical Feedback but not Both, The Astrophysical Journal, Volume 699, Issue 1, pp. 89-104 (2009).
- D'Onghia, Elena, et al., How galaxies lose their angular momentum, Monthly Notices of the Royal Astronomical Society, Volume 372, Issue 4, pp. 1525-1530.
- Eggen, O. J.; Lynden-Bell, D.; Sandage, A. R. Astrophysical Journal, vol. 136, p. 748.
- Elvis, M., et al., The Chandra COSMOS Survey. I. Overview and Point Source Catalog, The Astrophysical Journal Supplement, Volume 184, Issue 1, pp. 158-171 (2009).
- Fabbian, G.; Trinchieri, G.; MacDonald, A., X-ray observations of spiral galaxies. I -

Integrated properties, Astrophysical Journal, Part 1 (ISSN 0004-637X), vol. 284, Sept. 1, 1984, p. 65-74.

- Fall, S.M., Efstathiou, G., 1980. Monthly Notices of the Royal Astronomical Society 193, 189-206.
- Fan, Xiaohui, et al., A Survey of z>5.7 Quasars in the Sloan Digital Sky Survey. IV. Discovery of Seven Additional Quasars, The Astronomical Journal, Volume 131, Issue 3, pp. 1203-1209.
- Ferrarese, Laura, Beyond the Bulge: A Fundamental Relation between Supermassive Black Holes and Dark Matter Halos, The Astrophysical Journal, Volume 578, Issue 1, pp. 90-97.
- Ferrarese, Laura; Merrit, David, A Fundamental Relation between Supermassive Black Holes and Their Host Galaxies, The Astrophysical Journal, Volume 539, Issue 1, pp. L9-L12.
- Font, A. S., et al., Halo Substructure and Disk Heating in a Λ Cold Dark Matter Universe, The Astrophysical Journal, Volume 563, Issue 1, pp. L1-L4.
- Frenk, C.S., White, S.D.M., Davis, M., Efstathiou, G., 1988. Astrophysical Journal 327, 507-525.
- Governato, F., et al., Bulgeless dwarf galaxies and dark matter cores from supernova-driven outflows, Nature, Volume 463, Issue 7278, pp. 203-206 (2010).
- Grimm, H.-J.; Gilfanov, M; Sunyaev, R., High-mass X-ray binaries as a star formation rate indicator in distant galaxies, Monthly Notice of the Royal Astronomical Society, Volume 339, Issue 3, pp. 793-809.
- Haiman, Z., Constraints from Gravitational Recoil on the Growth of Supermassive Black Holes at High Redshift, The Astrophysical Journal, Volume 613, Issue 1, pp. 36-40.
- Hasinger, G. et al, The XMM-Newton Wide-Field Survey in the COSMOS Field. I. Survey Description, The Astrophysical Journal Supplement Series, Volume 172, Issue 1, pp. 29-37.
- Hogg, David W., Distance measures in cosmology, ARXIV, 1999astro.ph..5116H.
- Hopkins, Philip F., et al, Stellar feedback and bulge formation in clumpy discs, Monthly Notices of the Royal Astronomical Society, Volume 427, Issue 2, pp. 968-

978.

- Hoyle, F., 1949. in: Problems in Cosmical Aerodynamics, Central Air Documents Office Ohio.
- Katz, N., 1992. Astrophysical Journal 391, 502-517
- Katz, Neal; Gunn, James E. , Dissipational galaxy formation. I - Effects of gasdynamics , Astrophysical Journal 377, 365-381.
- Kazantzidis, S., et al., Cold Dark Matter Substructure and Galactic Disks. I. Morphological Signatures of Hierarchical Satellite Accretion, The Astrophysical Journal, Volume 688, Issue 1, pp. 254-276.
- Koekemoer, A., et al., The COSMOS Survey: Hubble Space Telescope Advanced Camera for Surveys Observations and Data Processing, The Astrophysical Journal Supplement Series, Volume 172, Issue 1, pp. 196-202.
- Kormendy, J., Kennicutt, R.C., 2004. Annual Review of Astronomy and Astrophysics 42, p.603-683.
- Lehmann, I., et al., The ROSAT Deep Survey. VI. X-ray sources and Optical identifications of the Ultra Deep Survey, Astronomy and Astrophysics, v.371, p.833-857 (2001).
- Longair, M. S., High Energy Astrophysics, Vol. I, Cambridge University Press.
- Mao, M. Y., et al., No Evidence for Evolution in the Far-infrared-Radio Correlation out to $z \sim 2$ in the Extended Chandra Deep Field South, The Astrophysical Journal, Volume 731, Issue 2, article id. 79, 10 pp.
- Mayer, L.; Governato, F.; Kaufmann, T, The formation of disk galaxies in computer simulations, Advanced Science Letters, vol. 1, p. 7-27.
- Messias, H. et al., A Multi-wavelength Approach to the Properties of Extremely Red Galaxy Populations. I. Contribution to the Star Formation Rate Density and Active Galactic Nucleus Content, The Astrophysical Journal, Volume 719, Issue 1, pp. 790-802 (2010).
- Mo, H. J.; Mao, Shude; White, Simon D. M., The formation of galactic disks, Monthly Notices of the Royal Astronomical Society, Volume 295, Issue 2, pp. 319-336.
- Mushotzky, R., Supermassive Black Holes in the Distant Universe, Kluwer

Academic Publishers, Dordrecht, The Netherlands, 2004, p.53, Chapter 2.

- Navarro, J. F. et al., The assembly of galaxies in a hierarchically clustering universe, Monthly Notices of the Royal Astronomical Society, Volume 275, Issue 1, pp. 56-66.
- Navarro, J., F., White, S. D. M., Simulations of dissipative galaxy formation in hierarchically clustering universes-2. Dynamics of the baryonic component in galactic haloes, Monthly Notices of the Royal Astronomical Society, vol. 267, no. 2, p. 401-412.
- Omukai, K., et al., Can Supermassive Black Holes Form in Metal-enriched High-Redshift Protogalaxies?, The Astrophysical Journal, Volume 686, Issue 2, pp. 801-814.
- Peebles, P. J. E. ,The Effect of a Lumpy Matter Distribution on the Growth of Irregularities in an Expanding Universe, Astronomy and Astrophysics, Vol. 32, p. 391 (1974)
- Peebles, P. J. E., Large Scale Structure of the Universe, 1980, Princeton University Press
- Ranalli, P.; Comastri, A.; Setti, G., The 2-10 keV luminosity as a Star Formation Rate indicator, Astronomy and Astrophysics, v.399, p.39-50 (2003).
- Robertson, B., et al., The Fundamental Scaling Relations of Elliptical Galaxies, The Astrophysical Journal, Volume 641, Issue 1, pp. 21-40.
- Schleicher, D. R. G.; Spaans, M.; Glover, S. C. O., Black Hole Formation in Primordial Galaxies: Chemical and Radiative Conditions, The Astrophysical Journal Letters, Volume 712, Issue 1, pp. L69-L72 (2010).
- Schmitt, H. R., et al., Ultraviolet-to-Far-Infrared Properties of Local Star-forming Galaxies, The Astrophysical Journal, Volume 643, Issue 1, pp. 173-185.
- Scoville, et al., The Cosmic Evolution Survey (COSMOS): Overview, The Astrophysical Journal Suplement, Volume 172, Issue 1, 2007.
- Sharma, S., Steinmetz, M., The Angular Momentum Distribution of Gas and Dark Matter in Galactic Halos, The Astrophysical Journal, Volume 628, Issue 1, 21-44.
- Spitzer, Lyman, Jr.; Schwarzschild, Martin, The Possible Influence of Interstellar Clouds on Stellar Velocities. II, Astrophysical Journal, vol. 118, p.106.

- Springel, Volker; Di Matteo, Tiziana; Hernquist, Lars, Modelling feedback from stars and black holes in galaxy mergers, Monthly Notices of the Royal Astronomical Society, Volume 361, Issue 3, pp. 776-794.
- Steinmetz, M., Navarro, J. F., The hierarchical origin of galaxy morphologies, New Astronomy, Volume 7, Issue 4, p. 155-160.
- Steinmetz, Matthias; Navarro, Julio F., The Cosmological Origin of the Tully-Fisher Relation, The Astrophysical Journal, Volume 513, Issue 2, pp. 555-560.
- Thacker, R. J., Couchman, H. M. P., Star Formation, Supernova Feedback, and the Angular Momentum Problem in Numerical Cold Dark Matter Cosmogony: Halfway There?, The Astrophysical Journal, Volume 555, Issue 1, pp. L17-L20.
- van den Bosch, et al., The Angular Momentum of Gas in Protogalaxies. I. Implications for the Formation of Disk Galaxies, The Astrophysical Journal, Volume 576, Issue 1, 21-35.
- Vattakunnel, S., et al, The radio-X-ray relation as a star formation indicator: results from the Very Large Array-Extended Chandra Deep Field-South, Monthly Notices of the Royal Astronomical Society, Volume 420, Issue 3, pp. 2190-2208.
- Walker, Ian R.; Mihos, J. Christopher; Hernquist, Lars, Quantifying the Fragility of Galactic Disks in Minor Mergers, The Astrophysical Journal v.460, p.121.
- White, S.D.M., Frenk, C.S., 1991. Astrophysical Journal 379, 52-79.
- Yi, Insu; Boughn, Stephen P, On Radio and X-ray Mechanics in Nearby, X-ray-bright Galactic Nuclei, The Astrophysical Journal, Volume 515, Issue 2, pp 576-582.
- Yun, M., S., et al., Radio Properties of Infrared-selected Galaxies in the IRAS 2 Jy Sample, The Astrophysical Journal, Volume 554, Issue 2, pp. 803-822.
- Zamojsky et al., Deep GALEX Imaging of the COSMOS HST Field: A First Look at the Morphology of z ~ 0.7 Star-forming Galaxies,The Astrophysical Journal Supplement Series, Volume 172, Issue 1, pp. 468-493.